





ARTICLE

<https://doi.org/10.1038/s41467-019-12868-1>

OPEN

# Cellular sequestrases maintain basal Hsp70 capacity ensuring balanced proteostasis

Chi-ting Ho<sup>1,2</sup>, Tomas Grousl <sup>1,2,3,4</sup>, Oren Shatz<sup>1,2,4</sup>, Areeb Jawed<sup>1,2,4</sup>, Carmen Ruger-Herreros <sup>1,2,4</sup>, Marije Semmelink<sup>1,2</sup>, Regina Zahn <sup>1,2</sup>, Karsten Richter<sup>2</sup>, Bernd Bukau <sup>1,2\*</sup> & Axel Mogk<sup>1,2\*</sup>

Maintenance of cellular proteostasis is achieved by a multi-layered quality control network, which counteracts the accumulation of misfolded proteins by refolding and degradation pathways. The organized sequestration of misfolded proteins, actively promoted by cellular sequestrases, represents a third strategy of quality control. Here we determine the role of sequestration within the proteostasis network in *Saccharomyces cerevisiae* and the mechanism by which it occurs. The Hsp42 and Btn2 sequestrases are functionally intertwined with the refolding activity of the Hsp70 system. Sequestration of misfolded proteins by Hsp42 and Btn2 prevents proteostasis collapse and viability loss in cells with limited Hsp70 capacity, likely by shielding Hsp70 from misfolded protein overload. Btn2 has chaperone and sequestrase activity and shares features with small heat shock proteins. During stress recovery Btn2 recruits the Hsp70-Hsp104 disaggregase by directly interacting with the Hsp70 co-chaperone Sis1, thereby shunting sequestered proteins to the refolding pathway.

<sup>1</sup>Center for Molecular Biology of Heidelberg University (ZMBH), Im Neuenheimer Feld 282, DKFZ-ZMBH Alliance, Heidelberg, Germany. <sup>2</sup>German Cancer Research Center (DKFZ), 69120 Heidelberg, Germany. <sup>3</sup>Present address: Institute of Microbiology of the Czech Academy of Sciences, Prague, Czech Republic. <sup>4</sup>These authors contributed equally: Tomas Grousl, Oren Shatz, Areeb Jawed, Carmen Ruger-Herreros. \*email: [bukau@zmbh.uni-heidelberg.de](mailto:bukau@zmbh.uni-heidelberg.de); [a.mogk@zmbh.uni-heidelberg.de](mailto:a.mogk@zmbh.uni-heidelberg.de)

The cellular network that maintains protein homeostasis (proteostasis) has long been considered to rely on two main strategies: to promote the refolding of misfolded proteins by molecular chaperones and to degrade them by proteolytic systems. The cellular capacity to pursue these strategies, however, becomes limited under severe protein folding stress and declines during aging, ultimately resulting in increased protein aggregation<sup>1–4</sup>. The accumulation of aggregates has therefore been viewed as a hallmark of proteostasis collapse, and aggregation as uncontrolled process of denatured proteins that clump together via hydrophobic interactions.

This view has recently changed due to several lines of observations. The aggregation of proteins under severe heat stress is not random, but mainly involves proteins that function in protein synthesis (e.g. translation), and hence constitutes a cellular response to control the flux of newly synthesized proteins into the proteome<sup>5,6</sup>. Misfolded proteins are deposited at inclusions located to specific cellular sites<sup>7–9</sup>, through a process that depends on dedicated molecular chaperones, termed sequestrases<sup>8,10–15</sup>. Hence, “protein aggregation” under these conditions is the result of a regulated cellular process, and represents an organized sequestration event.

In *Saccharomyces cerevisiae* Hsp42 and Btn2 promote protein sequestration during moderate heat stress, genotoxic stress and cellular aging<sup>11–17</sup>. Hsp42 and Btn2 act largely compartment-specific by controlling sequestrations in the cytosol (CytQ, Q-bodies) and nucleus (INQ), respectively. Both chaperones additionally undergo inter-compartmental cross-talk, affecting protein sequestration in the other compartment<sup>13,17</sup>. Hsp42 is a member of the small heat-shock protein (sHsp) family and harbours a disordered prion-like domain (PrLD) that is essential for sequestrase function<sup>18</sup>. In contrast, Btn2 is largely uncharacterized.

The sequestration of misfolded proteins is now recognized as the third strategy of the proteostasis network, helping cells to cope with an overload of misfolded proteins<sup>19–21</sup>. But how important sequestrases exactly are in relation to the two other proteostasis strategies, and to what extent they contribute to the buffering of cytotoxicity induced by misfolding has remained elusive. Several beneficial consequences of sequestrase activities have been suggested. First, sequestration of misfolded proteins confines their accessible sticky surface, thereby eventually reducing cytotoxicity<sup>1,22–26</sup>. This might also, secondly, prevent exhaustion of finite resources of chaperone and protease systems. Third, the formation of protein sequestrations can facilitate asymmetric inheritance of damaged proteins, allowing for formation of aggregate-free daughter cells<sup>27–29</sup>. Fourth, the spatial concentration of misfolded proteins through sequestration might aid chaperone and proteolytic activities to facilitate repair or clearance<sup>30</sup>. Whether and how sequestrases target sequestered substrates to refolding or proteolytic pathways is unknown. A major limitation in analysing sequestrase function experimentally has been the absence of strong growth phenotypes of respective mutant cells.

Here we dissect the function and mechanism of Hsp42- and Btn2-mediated, organized protein sequestration for stress biology of yeast cells. We show that the Hsp42 and Btn2 become essential for cell growth upon confining Hsp70 capacity, by ensuring basal Hsp70 activity and preventing proteostasis collapse. We biochemically define Btn2 domains that execute distinct functions in both protein sequestration during stress and recruiting Hsp70/Hsp100 disaggregases for refolding of sequestered proteins during stress recovery. Our findings imply that the two sequestrases constitute a stress rescue system that is essential for viability upon misfolded protein overload, by mitigating the burden on the Hsp70 chaperone machinery.

## Results

**Sequestrases become crucial in cells with low Hsp70 capacity.** Btn2 and Hsp42 organize protein sequestration in *S. cerevisiae* cells. However, respective knockout cells do not show pronounced growth defects under stress conditions<sup>13</sup>. We hypothesized that the absence of a strong phenotype results from compensatory activities of other proteostasis components involved in protein folding or degradation pathways, superseding the need for sequestrases. Accordingly, sequestrases might become important in cells with reduced proteolytic or refolding capacities. We therefore screened for synthetic sickness of *btn2Δ* and *hsp42Δ* cells in mutant backgrounds with reduced proteasome or chaperone activities.

To lower proteasome activity we used *rpn4Δ* and *irc25Δ* knockouts, which are compromised in expression of proteasomal genes and 26S proteasome assembly, respectively<sup>31,32</sup>. The mutations result in reduced levels of 26S proteasomes and temperature-sensitive growth<sup>33</sup> (Supplementary Fig. 1a). Additionally, we employed *rsp5-3* and *ubr1Δ/san1Δ* mutants, which lack E3 ligases that play key roles in the ubiquitination and degradation of misfolded proteins<sup>34–37</sup>. We did not observe increased temperature sensitivity when deleting *btn2* or *hsp42* in these mutants, suggesting that degradation and sequestration of heat-induced misfolded proteins are not interlocked in a phenotypically apparent manner (Supplementary Fig. 1a).

We next tested for an interconnection between Btn2/Hsp42 and the Hsp70 system, which is a central component of the proteostasis network<sup>38,39</sup>. We employed several strategies to reduce the capacity of the four cytosolic/nuclear Hsp70 chaperones, Ssa1–4, which collectively are essential (Fig. 1a, Supplementary Fig. 1b). First, we deleted the *ssa1* and *ssa2* genes encoding for the two major Ssa's, but did not observe synthetic sickness when linking *ssa1Δ ssa2Δ* to *btn2Δ* or *hsp42Δ* (Supplementary Fig. 1b). Second, we employed deletions of genes encoding the Hsp70 partner chaperones Sse1, Fes1 and Hsp104. Fes1 and Sse1 function as nucleotide exchange factors (NEFs) of Ssa's, catalysing ADP to ATP exchange, which promotes dissociation of bound substrates<sup>40</sup>. The AAA + chaperone Hsp104 cooperates with Hsp70 in protein disaggregation, taking over Ssa-bound substrates through direct Ssa-Hsp104 interaction<sup>41,42</sup>. In the respective mutant cells, Ssa-substrate interactions will therefore be stabilized, reducing the available pool of cytosolic/nuclear Hsp70 chaperones, and hence the cellular Hsp70 capacity (Fig. 1b). Third, we depleted the essential J-protein Sis1 in the presence and absence of Hsp42 and Btn2. Depletion of Sis1 will lower Hsp70 activity and hamper Hsp70-dependent folding processes.

We observed severe synthetic growth defects at 30 °C when deleting *btn2* in *fes1Δ hsp104Δ* (also referred to as  $\Delta\Delta$ ) mutant cells, but not in other mutant combinations (i.e. *sse1Δ fes1Δ* and *sse1Δ hsp104Δ*) (Fig. 1a, Supplementary Fig. 1b). Deleting *hsp42* in *sse1Δ hsp104Δ* mutants also caused a temperature-sensitive growth phenotype at 37 °C (Supplementary Fig. 1b). Furthermore, lowering Sis1 levels by placing it under the control of a doxycycline-repressible promoter caused synthetic sickness at high temperatures (37 °C/39 °C) when combined with *btn2Δ* and *hsp42Δ* knockouts (Supplementary Fig. 1d, e). Altogether, these findings manifest that sequestrases become crucial in cells with low Hsp70 activity. Since  $\Delta\Delta$  *btn2Δ* cells exhibited the strongest growth deficiencies, we focussed our analysis on those cells.

At 33 °C we also observed synthetic sickness when deleting *hsp42* in  $\Delta\Delta$  cells (Fig. 1a). A quadruple knockout  $\Delta\Delta$  *btn2Δ hsp42Δ* (also referred to as  $\Delta\Delta\Delta\Delta$ ) did not increase temperature sensitivity further. This suggests a dominant function of Btn2 in cell protection under Hsp70-limited conditions. Synthetic sickness of  $\Delta\Delta$  *btn2Δ*,  $\Delta\Delta$  *hsp42Δ* and  $\Delta\Delta$  *btn2Δ*

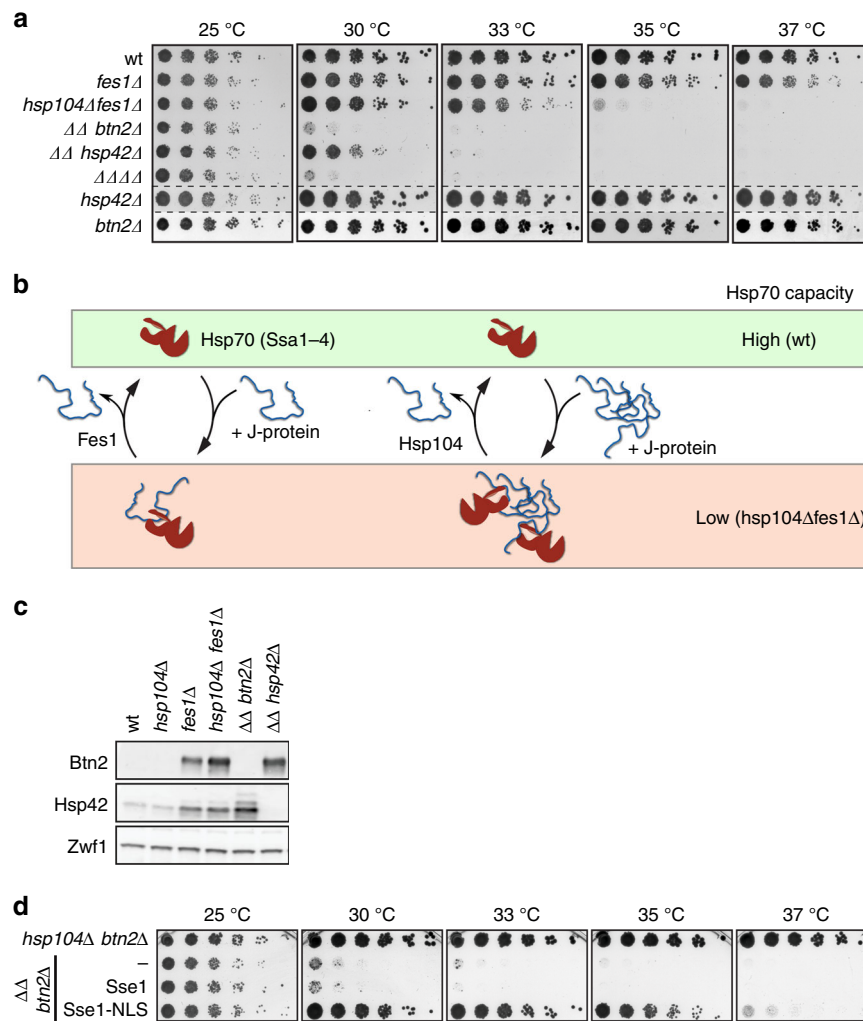


**Fig. 1** Btn2 becomes essential for cell growth upon confining nuclear Hsp70 capacity. **a** Serial dilutions of indicated *S. cerevisiae* wild type (wt) and chaperone mutant cells ( $\Delta\Delta$ : *hsp104Δ fes1Δ*;  $\Delta\Delta\Delta$ : *hsp104Δ fes1Δ btn2Δ hsp42Δ*) were spotted on YPD plates and incubated at indicated temperatures for 2 days. **b** The nucleotide exchange factor Fes1 and the Hsp104 disaggregase displace Hsp70-bound substrates, thereby recycling Hsp70 and ensuring high Hsp70 capacity (wt cells). Lack of these Hsp70 co-chaperones in *hsp104Δ fes1Δ* cells cause low Hsp70 capacity. **c** Btn2 and Hsp42 levels were determined at 30 °C in *S. cerevisiae* wt and chaperone mutant cells by western blot analysis. Zw1 levels were determined as a loading control. **d** Serial dilutions of indicated *S. cerevisiae* chaperone mutant cells were spotted on YPD plates and incubated at indicated temperatures for 2 days.  $\Delta\Delta$  *btn2Δ* cells expressed an additional copy of either Sse1 or Sse1-NLS, harbouring a C-terminal nuclear localization sequence

*hsp42Δ* was confirmed when growth curves of respective cells were recorded at different temperatures in liquid media (Supplementary Fig. 1c).

Why do *btn2Δ* cells specifically show a strong genetic interaction with *fes1Δ hsp104Δ* ( $\Delta\Delta$ ) cells?  $\Delta\Delta$  cells exhibit the strongest temperature sensitivity when compared to all other Hsp70 mutant strains tested, suggesting that Hsp70 capacity is particularly low in these cells (Supplementary Fig. 1b). Btn2 levels were particularly high in  $\Delta\Delta$  cells, consistent with high activity of the heat-shock transcription factor Hsf1 (which controls *btn2* expression) resulting from low Hsp70 activity, which negatively regulates Hsf1 function (Fig. 1c, Supplementary Fig. 2a)<sup>43,44</sup>. In line with an HSF1-mediated heat-shock response, the levels of Hsp42 (Fig. 1c) and other chaperones (e.g. Ssa1–4, Hsp26) (Supplementary Fig. 2b) were high in  $\Delta\Delta$  and further increased (Hsp42, Hsp26) in  $\Delta\Delta$  *btn2Δ* cells. We directly demonstrate activation of the heat-shock response in  $\Delta\Delta$  cells by use of a *gfp* reporter gene placed under control of Hsf1 (Supplementary Fig. 2c). This automatic increase of Btn2 but also Hsp42 levels in the Hsp70 mutant background explains how the sequestrases can

increase their capacity and thereby act as efficient rescue system to maintain cell growth. Notably, the increased expression of other Hsf1-dependent chaperones does not rescue the growth defect of  $\Delta\Delta$  *btn2Δ* cells, documenting that  $\Delta\Delta$  cells are particularly dependent on sequestrase activity.

An increased temperature sensitivity was not observed when introducing the *btn2Δ* allele in single *fes1Δ* or *hsp104Δ* mutant cells, although *fes1Δ btn2Δ* cells formed smaller colonies as compared to respective single knockouts, indicating minor synthetic growth defects (Supplementary Fig. 2d). We also introduced the *hsp26Δ* allele into  $\Delta\Delta$  cells. Hsp26 is the second bona fide yeast sHsp, which, however, requires activation by heat stress and does not exhibit sequestrase activity<sup>11,45</sup>. We did not observe increased temperature sensitivity for  $\Delta\Delta$  *hsp26Δ* cells (Supplementary Fig. 2d). The Hsp90 chaperone system represents another major chaperone system of yeast cells that is essential for viability. When lowering Hsp90 activity upon addition of the Hsp90-specific inhibitor Radicolol, no synthetic growth defects were observed in *btn2Δ* cells (Supplementary Fig. 2e). Together, these findings indicate a functional interconnection specifically

between the Hsp70 chaperone system and the sequestrases Btn2 and Hsp42.

To further support an essential function of Btn2 for cell growth at reduced Hsp70 capacity, we sought to rescue growth of  $\Delta\Delta$  *btn2* $\Delta$  cells by re-increasing Hsp70 availability. First, we over-produced Ssa1 from plasmid p415GPD-Ssa1, increasing total Hsp70 levels by 2-fold; this only partially rescued growth of  $\Delta\Delta$  *btn2* $\Delta$  cells at 33 °C (Supplementary Fig. 3a, b). The weak complementation can be explained by the specific defect of  $\Delta\Delta$  cells in releasing the substrate from Hsp70, which is not overcome by Ssa1 overproduction.

To specifically rescue this deficiency of  $\Delta\Delta$  cells, we targeted Sse1, the major NEF for Ssa's<sup>46,47</sup> to the nucleus. Sse1 is largely excluded from the nucleus, whereas Fes1 is located in both the cytosol and the nucleus (Supplementary Fig. 3c)<sup>48,49</sup>.  $\Delta\Delta$  cells therefore lack the sole nuclear NEF, rationalizing growth dependence on nuclear Btn2. We expressed Sse1-NLS harbouring a C-terminal nuclear localization sequence (NLS) as additional copy at low levels in  $\Delta\Delta$  *btn2* $\Delta$  cells (Fig. 1d, Supplementary Fig. 3d). Sse1-NLS expression fully restored growth of  $\Delta\Delta$  *btn2* $\Delta$  cells up to 35 °C, demonstrating that re-increasing nuclear Hsp70 capacity overcomes growth dependence on Btn2. An NLS-tagged Sse1 mutant that harbours multiple mutations in its substrate binding site (Sse1<sub>SBD</sub>: L433A/N434P/F439/M441A) and is strongly affected in substrate binding<sup>50</sup> rescued growth of  $\Delta\Delta$  *btn2* $\Delta$  cells at 30 °C, supporting that NEF activity of Sse1 is most important (Supplementary Fig. 3e). Complementation activity of Sse1<sub>SBD</sub> was reduced at increased temperatures, suggesting that Sse1 chaperone activity also contributes to growth rescue in agreement with former findings<sup>50</sup>.

**Lack of sequestrase activities causes proteostasis collapse.** We set out to directly link the determined growth deficiencies of  $\Delta\Delta$  *btn2* $\Delta$  and  $\Delta\Delta$  *hsp42* $\Delta$  cells to alterations in proteostasis. To monitor protein sequestration patterns in these mutants, we tested the intracellular localization of the constitutively misfolded reporter GFP-VHL<sup>7</sup>. As compared to wild type (wt), the levels of GFP-VHL were increased to similar degrees in all mutant cells tested ( $\Delta\Delta$ ,  $\Delta\Delta$  *btn2* $\Delta$ ,  $\Delta\Delta$  *hsp42* $\Delta$ ,  $\Delta\Delta\Delta\Delta$ ) (Supplementary Fig. 3f), consistent with the previously reported role of the Hsp70 system in the degradation of soluble VHL<sup>51</sup> and the limited Hsp70 capacity in the mutants. At 25 °C, GFP-VHL showed diffuse fluorescence in wt, but formed nuclear foci (INQ) in a subset (11%) of  $\Delta\Delta$  cells (Fig. 2a, b). GFP-VHL foci were not observed in  $\Delta\Delta$  *btn2* $\Delta$  and  $\Delta\Delta$  *hsp42* $\Delta$  cells, indicating that foci formation results from an active, Hsp42- or Btn2-mediated sequestration process and not from a general proteostasis collapse. Co-localization of Btn2 and GFP-VHL foci in  $\Delta\Delta$  cells confirmed a direct role of Btn2 for the sequestration (Supplementary Fig. 3g). A puzzling finding is the absence of nuclear INQ formation in  $\Delta\Delta$  *hsp42* $\Delta$  cells (Fig. 2a). This suggests that the activities of cytosolic and nuclear sequestrases, Hsp42 and Btn2, respectively, can be interdependent in agreement with former findings<sup>17,52</sup>. The basis of this relationship is currently unknown and the inter-dependence as described here was not observed earlier when applying more severe proteotoxic stress<sup>13</sup>.

We next monitored the short- and long-term consequences of preventing organized protein sequestration in  $\Delta\Delta$  *btn2* $\Delta$  and  $\Delta\Delta$  *hsp42* $\Delta$  cells by exposing the cells to non-permissive growth conditions (30 °C). Shifting  $\Delta\Delta$  cells from 25 °C to 30 °C for 60 min increased the fraction of cells harbouring nuclear GFP-VHL foci (INQ) from 11 to 32% and this number further increased to 49% upon 8-h incubation (Fig. 2a, b);  $\Delta\Delta$  cells additionally harboured 1–2 cytosolic GFP-VHL foci (CytoQ) (60 min: 15%, 8 h: 29%). At the initial phase (60 min) of temperature upshift, GFP-VHL

sequestration was not observed in  $\Delta\Delta$  cells, additionally lacking either Btn2 or Hsp42 (Fig. 2a, b). Prolonged incubation at non-permissive conditions, however, caused splitting of  $\Delta\Delta$  *btn2* $\Delta$ ,  $\Delta\Delta$  *hsp42* $\Delta$  and  $\Delta\Delta$  *hsp42* $\Delta$  *btn2* $\Delta$  cells into two populations showing differing GFP-VHL localization patterns. While in 76% of  $\Delta\Delta$  *btn2* $\Delta$  cells GFP-VHL fluorescence remained diffuse, 21% of cells showed large, multiple (>3) GFP-VHL foci in the cytosol and no diffuse fluorescence, indicating protein aggregation and proteostasis collapse (Fig. 2a, b). Similar results were obtained when analysing  $\Delta\Delta$  *hsp42* $\Delta$  and  $\Delta\Delta$  *hsp42* $\Delta$  *btn2* $\Delta$  cells (Fig. 2a, b).

We also analysed whether aggregation of GFP-VHL can be observed upon loss of Hsp42 sequestrase function in *sse1* $\Delta$  *hsp104* $\Delta$  mutant cells, which leads to a temperature-sensitive growth phenotype at 35–37 °C (Supplementary Fig. 1b). Shifting *sse1* $\Delta$  *hsp104* $\Delta$  *hsp42* $\Delta$  cells to 37 °C caused uncontrolled aggregation of GFP-VHL, whereas *sse1* $\Delta$  *hsp104* $\Delta$  control cells showed diffuse fluorescence or CytoQ formation (Supplementary Fig. 3h, i). We infer that loss of sequestrase function in these cells ultimately results in uncontrolled and harmful protein aggregation. This supports a critical role of Btn2 and Hsp42 in maintaining cellular proteostasis in cells with limited Hsp70 capacity.

**Btn2 and Hsp42 maintain basal levels of Hsp70 capacity.** To directly monitor the status of Hsp70 activity as a foldase in the diverse mutant strains, we made use of Luciferase-DM (R188Q/R261Q), a hyper-thermolabile variant of the Hsp70 substrate firefly Luciferase<sup>3,53</sup>. We genetically fused Luciferase-DM with GFP allowing to correlate Luciferase activity with subcellular localization and sequestration. Since the nuclear compartment is particularly vulnerable towards loss of sequestrase (Btn2) activity (Figs. 1a, 2a), we targeted the reporter to the nucleus by inserting the SV40 NLS, generating GFP-Luciferase-DM-NLS. At 25 °C Luciferase activities and levels were largely comparable for wt and all chaperone mutants tested (Fig. 2c). Upon continuous incubation at 28 and 30 °C, Luciferase activities remained stable in wt cells while, respectively, decreasing to 72% and 29% in  $\Delta\Delta$  cells, indicating deficiencies in Hsp70-dependent folding of GFP-Luciferase-DM-NLS (Fig. 2c). The drop of Luciferase activity at 30 °C in  $\Delta\Delta$  cells correlated with reduced levels as well as nuclear foci formation (INQ) of GFP-Luciferase-DM-NLS (Fig. 2d–f). This indicates that lowering Hsp70 capacity triages nuclear Luciferase towards both degradation and controlled sequestration pathways.

The temperature-dependent inactivation of Luciferase was further increased in  $\Delta\Delta$  *hsp42* $\Delta$  and  $\Delta\Delta$  *btn2* $\Delta$  cells, which displayed only 10% and 8% reporter activity at 30 °C, respectively (Fig. 2c). This further loss of activity was not caused by enhanced degradation as reporter levels were comparable to  $\Delta\Delta$  cells (Fig. 2d). However, instead of chaperone-dependent sequestration into nuclear deposits (INQ), we observed sequestrase-independent aggregation of GFP-Luciferase-DM-NLS as 86% of  $\Delta\Delta$  *btn2* $\Delta$  and 55% of  $\Delta\Delta$  *hsp42* $\Delta$  cells exhibited multiple, cytosolic GFP-Luciferase-DM-NLS foci (Fig. 2e, f). Diffuse nuclear reporter staining, still detectable in  $\Delta\Delta$  cells, was hardly observed in the triple mutants, explaining the extensive loss of Luciferase activity in, for example, the  $\Delta\Delta$  *btn2* $\Delta$  mutant cells. When comparing the time-resolved changes in GFP-Luciferase-DM-NLS localization in  $\Delta\Delta$  and  $\Delta\Delta$  *btn2* $\Delta$  cells upon temperature upshift from 25 to 30 °C, we observed that controlled, Btn2-dependent INQ formation in  $\Delta\Delta$  cells preceded the formation of multiple foci in  $\Delta\Delta$  *btn2* $\Delta$  cells (Fig. 2g). We infer that loss of the Btn2-dependent GFP-Luciferase-DM-NLS sequestration immediately after shift to non-permissive conditions causes proteostasis breakdown and uncontrolled reporter aggregation, leading to lower levels of native protein.

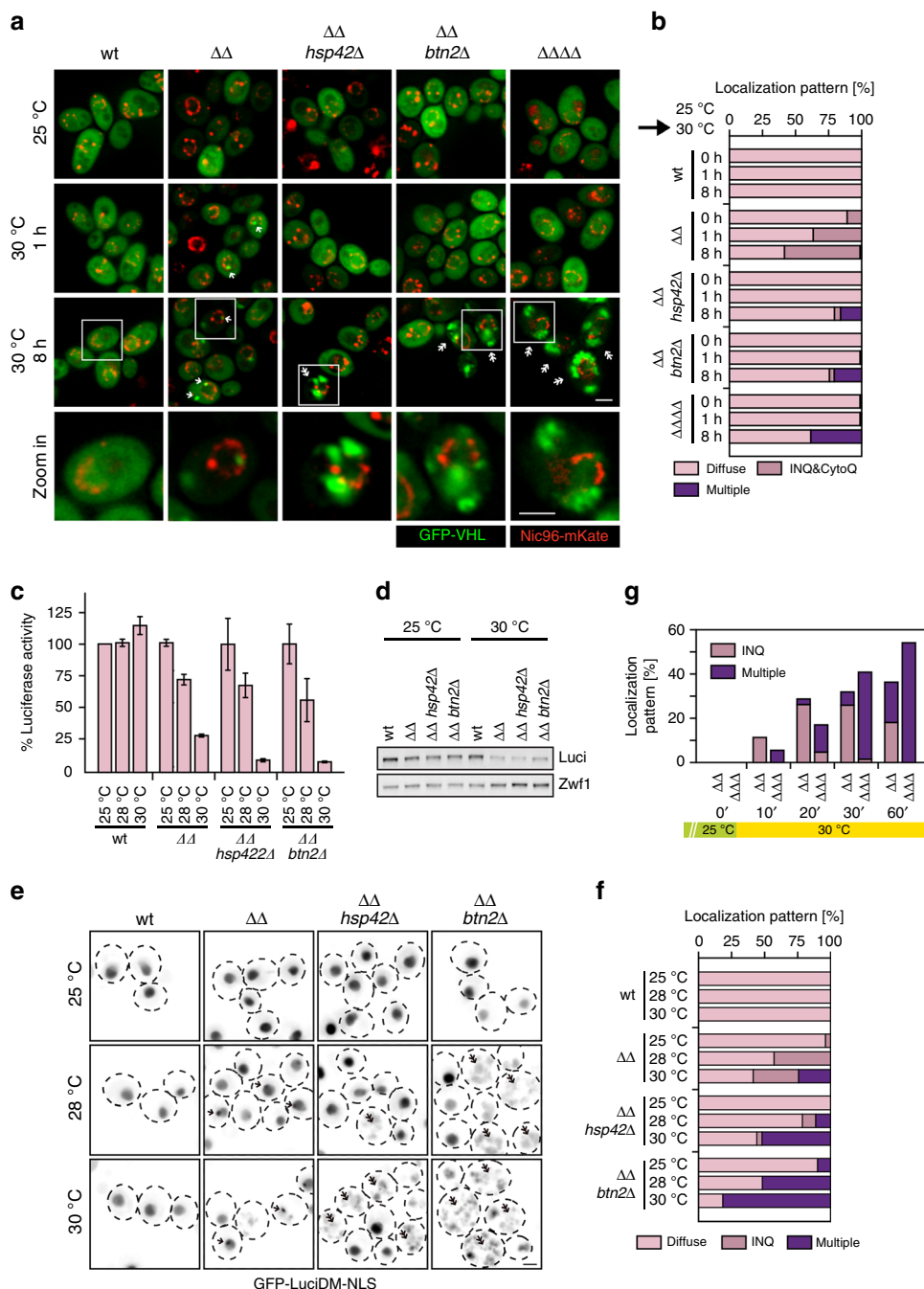


**Fig. 2** Loss of Btn2 causes proteostasis collapse. **a, b** *Saccharomyces cerevisiae* wild type (wt) and indicated chaperone mutant cell ( $\Delta\Delta$ : *hsp104Δ fes1Δ*;  $\Delta\Delta\Delta\Delta$ : *hsp104Δ fes1Δ btn2Δ hsp42Δ*) expressing the misfolded reporter GFP-VHL were grown at 25 °C to mid-exponential growth phase and shifted to 30 °C for 1 and 8 h. The cellular localization of GFP-VHL was determined and quantified ( $n > 100$ , 2 replicates). The nuclear envelope was labelled by coexpression of fluorescent Nic96-mKate2 nucleoporin. INQ (1 GFP-VHL foci) and CytoQ (1–2 GFP-VHL foci) are located inside and outside the nucleus (single arrow). Massive GFP-VHL aggregation leads to the formation of multiple ( $n > 3$ ) GFP-VHL foci (double arrow). **c–f** *Saccharomyces cerevisiae* wild type (wt) and indicated chaperone mutant cells expressing GFP-LuciDM-NLS were grown in SC medium at indicated temperatures. Luciferase activities (**c**), levels (**d**) and cellular localizations (**e, f**) were determined. Luciferase activities were normalized to cell numbers and the activity determined in wt cells at 25 °C was set to 100% (**c**). Standard deviations were calculated based on three independent experiments. Levels of GFP-LuciDM-NLS were determined by western blot analysis. A Zwif1 loading control is provided (**d**). GFP-LuciDM-NLS localizations were quantified for  $n = 100$  cells (2 replicates). INQ foci (single arrow) are located at the rim of the nucleus stained by diffuse GFP-LuciDM-NLS and cells suffering from proteostasis collapse (multiple GFP-LuciDM-NLS foci) are marked by double arrow (**e, f**). **g** *Saccharomyces cerevisiae* *hsp104Δ fes1Δ* ( $\Delta\Delta$ ) and *hsp104Δ fes1Δ btn2Δ* ( $\Delta\Delta\Delta\Delta$ ) cells expressing GFP-LuciDM-NLS were grown at 25 °C and shifted to 30 °C. Cellular localizations of GFP-LuciDM-NLS were monitored and the fraction of cells showing single INQ and multiple ( $n > 3$ ) cytosolic foci were determined at the indicated time points ( $n = 50$ , 2 replicates)

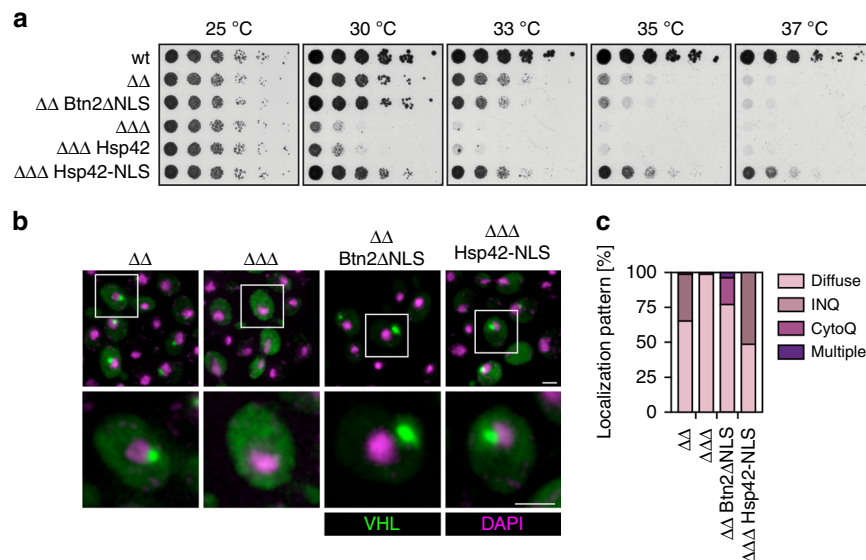


**Fig. 3** Sequestrase function per se is crucial for growth of *hsp104Δ fes1Δ* cells. **a** Serial dilutions of indicated *S. cerevisiae* wild-type (wt) and chaperone mutant cells ( $\Delta\Delta$ : *hsp104Δ fes1Δ*;  $\Delta\Delta\Delta$ : *hsp104Δ fes1Δ btn2Δ*) expressing Btn2 $\Delta$ NLS or Hsp42-NLS were spotted on YPD plates and incubated at indicated temperatures for 2 days. **b, c** *Saccharomyces cerevisiae* chaperone mutant cells expressing GFP-VHL or mCherry-VHL were grown at 25 °C. DNA was stained by DAPI. Cellular localizations of VHL were determined ( $n = 100$ ; 2 replicates). INQ and CytoQ foci were quantified depending on their position relative to the DAPI signal (INQ: directly adjacent; CytoQ: separated) by visual inspection

**Executors and sites of sequestration are interchangeable.** GFP-VHL is predominantly deposited in the nucleus of  $\Delta\Delta$  cells (Fig. 2a, b). Accordingly,  $\Delta\Delta$  *btn2Δ* cells are more temperature sensitive for growth as compared to  $\Delta\Delta$  *hsp42Δ* cells (Fig. 1a), suggesting a particular role of Btn2-driven INQ formation in cellular protection. We questioned whether the site of sequestration (nucleus vs. cytosol) and the implicated sequestration factor (Btn2 vs. Hsp42) are crucial for viability of  $\Delta\Delta$  cells. We therefore analysed whether  $\Delta\Delta$  *btn2Δ* cells can be rescued by (i) targeting the cytosolic Hsp42 to the nucleus (Hsp42-NLS) or (ii) directing misfolded proteins to cytosolic deposition sites by expressing Btn2- $\Delta$ NLS lacking its NLS as sole Btn2 copy (Fig. 3a, Supplementary Fig. 4a). Consequences on protein sequestration upon expression of Hsp42-NLS and Btn2- $\Delta$ NLS were monitored by use of the GFP-VHL reporter (Fig. 3b, c).

The presence of the *hsp42-NLS*, but not the *hsp42* allele, fully complemented growth deficiencies of  $\Delta\Delta$  *btn2Δ* cells, which even grew better than  $\Delta\Delta$  cells (Fig. 3a). Growth rescue correlated with the ability of Hsp42-NLS to efficiently restore nuclear deposition of GFP-VHL (Fig. 3b, c). To demonstrate that it is the sequestrase activity of Hsp42 that specifically rescues growth, we (i) expressed  $\Delta$ PrLD-*hsp42-NLS*, lacking the PrLD, which is essential for Hsp42 sequestrase activity<sup>18</sup> in  $\Delta\Delta$  *btn2Δ* cells or (ii) targeted Hsp26 to the nucleus of the mutant cells (Supplementary Fig. 4).  $\Delta$ PrLD-Hsp42-NLS did neither restore growth nor INQ formation (Supplementary Fig. 4b, c). Similarly, expressing *hsp26-NLS* as additional copy did not rescue growth and did not induce INQ formation, documenting specificity for Hsp42 sequestrase function (Supplementary Fig. 4b, d). We cannot exclude that the C-terminal NLS fusion alters Hsp26 oligomerization and functionality, although it does not affect Hsp42 (Fig. 3). Hsp26 is overproduced in *sse1Δ hsp104Δ hsp42Δ* cells, yet cannot compensate for the lack of the cytosolic sequestrase Hsp42 (Supplementary Fig. 4e). This further underlines that Hsp42, but not Hsp26, functions as sequestrase to protect cells under conditions of low Hsp70 capacity.

Growth of  $\Delta\Delta$  *btn2-ΔNLS* cells was indistinguishable from  $\Delta\Delta$  cells, but exhibited cytosolic instead of nuclear GFP-VHL inclusions (Fig. 3). Therefore, sequestrase function of Btn2-

$\Delta$ NLS in the cytosol is sufficient to rescue growth. We infer misfolded protein sequestration as such is most important to maintain growth of  $\Delta\Delta$  cells; the particular sequestrase (Btn2 vs. Hsp42) and sequestration sites (nucleus vs. cytosol) for misfolded proteins are in principle interchangeable. Notably, Hsp42-NLS but not Hsp42 triggers misfolded protein sequestration in  $\Delta\Delta$  *btn2Δ* cells. This might be explained by a higher local concentration due to the restricted space in the nucleus.

**Btn2 is a stand-alone sequestrase with sHsp-like features.** Btn2 represents an uncharacterized protein, which precludes further functional comparison with Hsp42. Moreover, the notable impact of Hsp42 on Btn2-driven sequestration of misfolded proteins in the nucleus (Fig. 2a, e) raises the question whether Btn2 alone can function as sequestrase. We therefore determined the biochemical properties and chaperone functions of purified Btn2 and compared them with those of Hsp42. We first analysed the oligomeric state of Btn2 by size-exclusion chromatography (Supplementary Fig. 5a). Btn2 eluted in the void volume indicating it forms high-molecular-weight complexes reminiscent of sHsp oligomers. Negative staining electron microscopy (EM) revealed that Btn2 forms globular structures with a diameter of 15–20 nm (Fig. 4a).

We next analysed the effects of Btn2 on aggregation of thermolabile Luciferase at 43 °C in vitro. Btn2 exhibits ATP-independent holdase activity and prevented the formation of large, turbid luciferase aggregates if present in 10-fold molar excess over substrate (Fig. 4b). This is reminiscent of sHsp chaperone activity including Hsp42, which prevented Luciferase aggregation if present in 5-fold molar excess. Btn2 association with misfolded Luciferase was confirmed by glycerol gradient centrifugation and negative staining EM showing the formation of smaller Btn2-Luciferase complexes (Fig. 4c, Supplementary Fig. 5b).

When shifting Btn2-Luciferase complexes, generated at 43 °C, back to 30 °C no spontaneous refolding of Luciferase was observed. This suggests that Btn2 stably sequesters Luciferase and does not release the substrate, similar to stable substrate binding by sHsps<sup>54</sup>. The stable nature of the sHsp-substrate

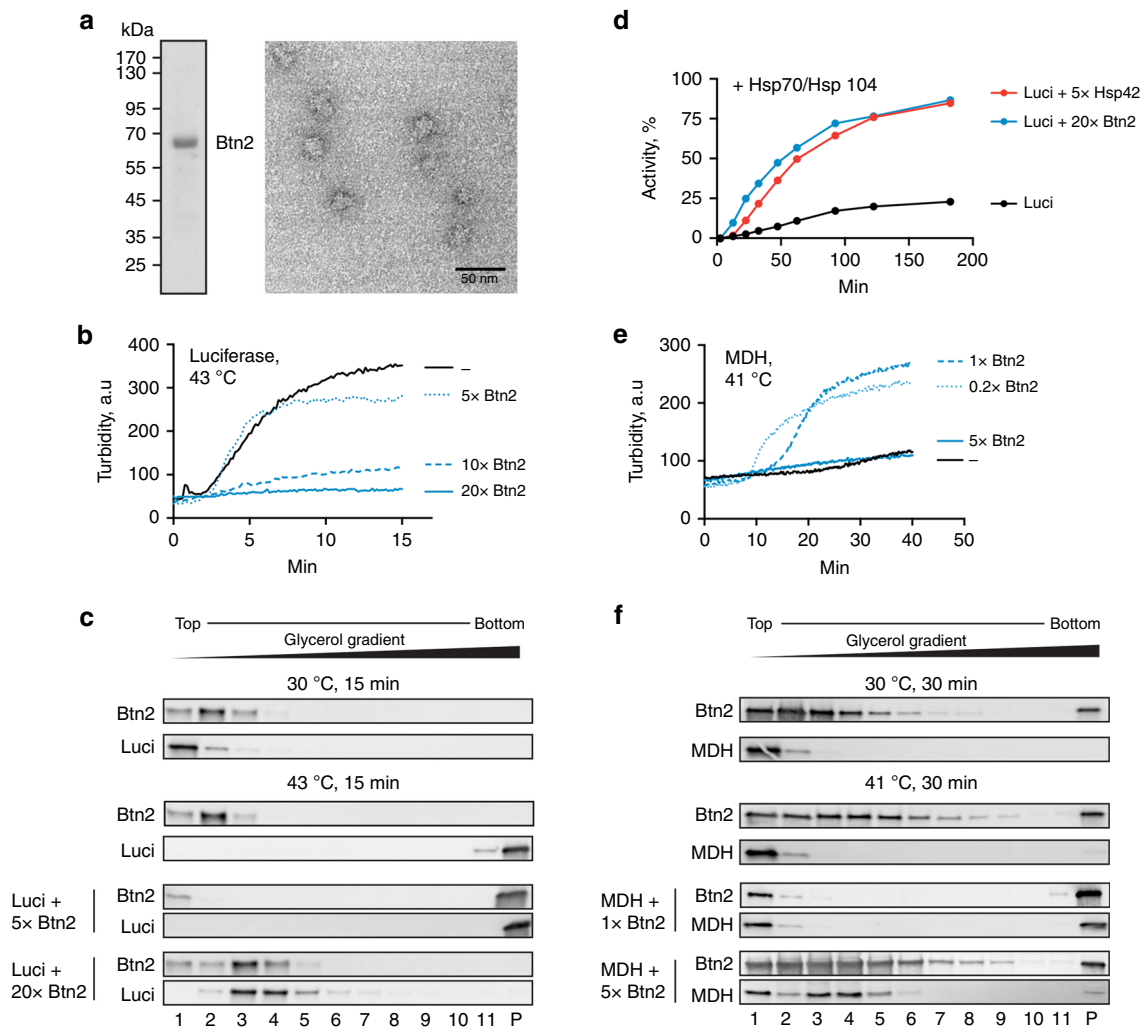


**Fig. 4** Btn2 has stand-alone chaperone and sequestrase activity. **a** The structure of purified Btn2 was analysed by negative stain electron microscopy. Scale bar: 50 nm. The purity of Btn2 (3  $\mu$ g) was documented by SDS-PAGE. Btn2 runs aberrantly, which might be caused by its highly charged C-terminal domain. **b, c** One hundred nanomolar Luciferase was incubated in the absence and presence of Btn2 at various ratios (0.5–2  $\mu$ M) at 43 °C and Luciferase aggregation was monitored by determining sample turbidity. A representative light scattering experiment is shown. Samples were additionally analysed by 10–50% glycerol gradient centrifugation and SDS-PAGE followed by western blot analysis. **d** Luciferase was aggregated at 43 °C for 15 min either alone or in the presence of a 5-fold and 20-fold excess of Hsp42 and Btn2, respectively. Luciferase activities were determined upon shifting the samples to 30 °C in the presence of the yeast bi-chaperone disaggregation system Hsp70/Hsp104 (Ssa1/Sis1/Fes1/Hsp104) and an ATP regenerating system. The activity of native Luciferase was set as 100%. A representative refolding experiment is shown. **e, f** Malate dehydrogenase (MDH) (0.5  $\mu$ M) was denatured at 41 °C in the absence or presence of Btn2 at various ratios (0.1–2.5  $\mu$ M). As control 2.5  $\mu$ M Btn2 was heated alone. Protein aggregation was monitored by determining sample turbidity and a representative light scattering experiment is shown. “–” (black line) refers to MDH-only sample. Samples were additionally analysed by glycerol gradient centrifugation as described above

complexes demands for Hsp70-Hsp100 disaggregase activity for substrate release and refolding<sup>54–57</sup>. Conversely, the binding of substrates to sHsps enhances refolding by disaggregases as compared to substrates aggregated in the absence of sHsps<sup>56,58,59</sup>. To assess whether Btn2 has similar features, we compared the reactivation of Luciferase from aggregated and Btn2-bound states by the yeast Hsp70 (Sis1/Ssa1/Fes1)–Hsp100 (Hsp104) bi-chaperone system. As a reference, we included Hsp42/Luciferase complexes, which allowed for 87% refolding of Luciferase within 180 min by the bi-chaperone system, while only 23% of Luciferase aggregated without Hsp42 was reactivated (Fig. 4d). Reactivation of Luciferase from soluble Btn2/Luciferase complexes by the Hsp70-Hsp100 bi-chaperone system (80% after 180 min) was comparable to that of Hsp42/Luciferase complexes, indicating that substrate sequestration by Btn2 also increases refolding yields (Fig. 4d). Notably, Btn2 also allowed for partial, Hsp104-

independent refolding of Luciferase by the Hsp70 system alone (Supplementary Fig. 5c), again revealing a chaperone activity similar to that of sHsps<sup>54</sup>. We conclude that Btn2 exhibits sHsp-like chaperone activity and associates with misfolded proteins to increase their reactivation by Hsp70-Hsp100 chaperones.

Btn2 is required for the formation of nuclear sequestrations in yeast cells<sup>13</sup>, while preventing protein aggregation in vitro (Fig. 4b, c). This seeming discrepancy either points to additional cellular factors required for nuclear sequestration of misfolded proteins or experimental limitations of the in vitro chaperone assays employed. We recently established an assay using malate dehydrogenase (MDH) as thermolabile substrate, which allowed to document sequestrase activity of Hsp42 in vitro<sup>45</sup>. Here, MDH is incubated at mild denaturing temperature (41 °C) well below its melting temperature (50.9 °C). This experimental parameter mimics more closely the moderate heat stress regimes imposed

onto cells when sequestrase activity is observed<sup>11–13</sup>. Incubation at 41 °C caused slow MDH unfolding without leading to the formation of turbid MDH aggregates (Fig. 4e, f, Supplementary Fig. 4d) in agreement with former findings<sup>45</sup>. The presence of sub-stoichiometric (1:0.2) and stoichiometric (1:1) MDH:Btn2 molar ratios triggered MDH “aggregation” and formation of turbid, insoluble MDH/Btn2 complexes (Fig. 4e, f). Btn2 did not accelerate MDH inactivation, excluding the possibility that Btn2 stimulates MDH “aggregation” by promoting MDH unfolding (Supplementary Fig. 5d). The addition of a high 5-fold molar excess of Btn2 led to the formation of non-turbid MDH/Btn2 complexes that were still larger as compared to MDH denatured in Btn2 absence (Fig. 4f). These findings indicate that the ratio between Btn2 and substrate is a key parameter to control the size of Btn2/substrate complexes, similar to what we observed for Hsp42<sup>45</sup>. Btn2 became an integral part of the complexes, demonstrating that Btn2 sequestrase activity involved direct physical interactions with misfolded MDH (Fig. 4f).

We infer that Btn2 exhibits functional similarities with Hsp42. Btn2 is necessary and sufficient to trigger sequestration of a denatured model substrate. Additional cellular factors are therefore not required to allow Btn2 to sequester proteins in vivo.

### Dissection of Btn2 domains crucial for sequestrase function.

Individual Btn2 domains have not been assigned and structural data are not available, hampering mechanistic analysis of Btn2-mediated protein aggregation. To define domains of Btn2, we first performed structure prediction by hidden Markov model (HMM)–HMM comparison (HHpred)<sup>60</sup>. HHpred revealed that, as best hit in the PDB (Protein Data Bank) database, the central segment of Btn2 comprising residues 101–218 shows a weak predicted secondary structure similarity to the conserved  $\alpha$ -crystallin domain of sHsps (Supplementary Fig. 6a). In similarity to  $\alpha$ -crystallin domains, this segment is predicted to consist of seven  $\beta$ -sheets, which led us to refer to it as  $\alpha$ -crystallin-like domain ( $\alpha$ CLD). The identification of the central  $\alpha$ CLD defines additional N-terminal (NTD, 1–100) and C-terminal (CTD, 218–410) domains for which, however, no related structure could be predicted (Fig. 5a). The NTD harbours the monopartite NLS (39KRRK42) of Btn2. Prediction of disordered and folded protein segments using IUPred<sup>61</sup> suggests that the NTD and  $\alpha$ CLD form folded structures, whereas the CTD is intrinsically disordered. This can be explained by low abundance of hydrophobic/aromatic amino acids (16.8%) and high content of charged residues (41.9%) in the CTD (Fig. 5a). Limited proteolysis of purified Btn2 by Subtilisin, which non-specifically cuts exposed protein segments, confirmed the predicted Btn2 domain organization. Subtilisin treatment generated two N-terminal Btn2 fragments comprising NTD (1–100) and NTD- $\alpha$ CLD (1–234) while causing rapid degradation of the CTD (Fig. 5b).

To identify domains critical for Btn2 sequestrase function, we created Btn2 deletion variants (Btn2- $\Delta$ NTD, Btn2- $\Delta$  $\alpha$ CLD, Btn2- $\Delta$ CTD) and C terminally fused the strong SV40 NLS to all constructs. Btn2-wt or deletion variants were expressed from the endogenous chromosomal locus in *hsp42 $\Delta$*  cells co-expressing the mCherry-VHL reporter. This facilitated the functional readout as mCherry-VHL is only deposited at nuclear INQ sites in these cells (Fig. 5c)<sup>11,13</sup>. All constructs additionally harboured a C-terminal FLAG-tag for quantification in western blots. We found comparable production of Btn2 constructs after heat shock except Btn2- $\Delta$ CTD, which accumulated to lower levels (Supplementary Fig. 5c). mCherry-VHL accumulated to comparable levels in all *btn2* mutant constructs tested (Supplementary Fig. 6b). Upon proteotoxic stress (37 °C + MG132), mCherry-VHL stayed diffuse in *hsp42 $\Delta$  btn2 $\Delta$*  cells, while Btn2-FLAG

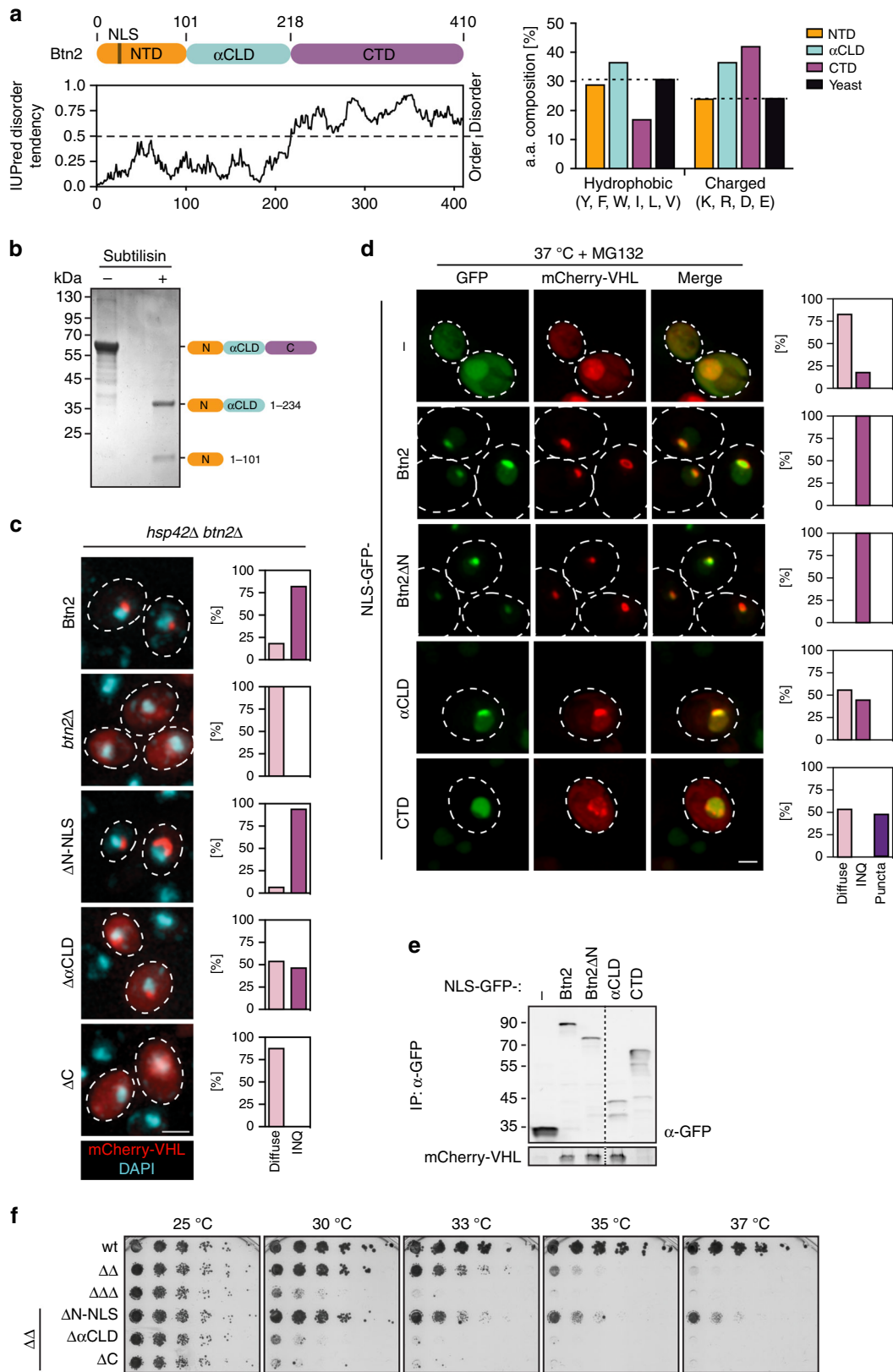
expression led to the formation of mCherry-VHL INQ foci (Fig. 5c, Supplementary Fig. 6c). Btn2- $\Delta$ NTD-NLS also efficiently triggered INQ formation, demonstrating that the NTD is dispensable for sequestrase function. In contrast deletions of  $\alpha$ CLD and CTD affected Btn2 sequestrase activity (Fig. 5c). mCherry-VHL stayed diffuse in cells expressing Btn2- $\Delta$ CTD and also did not form INQ in the majority (54%) of cells expressing Btn2- $\Delta$  $\alpha$ CLD. The remaining 46% of cells showed nuclear mCherry-VHL foci, but diffuse mCherry-VHL fluorescence was still observed in these cells, indicating inefficient INQ formation (Fig. 5c).

To further define roles of Btn2  $\alpha$ CLD and CTD in INQ formation, we performed a complementary approach and constitutively expressed the individual domains fused to GFP in yeast *hsp42 $\Delta$  btn2 $\Delta$*  cells. GFP fusions were tested for their ability to sequester mCherry-VHL at INQ. All GFP fusions harboured an additional N-terminal NLS ensuring nuclear localization and were produced at levels similar or higher as compared to GFP-Btn2 (Supplementary Fig. 6d). mCherry-VHL formed nuclear foci already at 30 °C in cells expressing GFP-Btn2, but not in cells expressing GFP fusions to single  $\alpha$ CLD and CTD domains (Supplementary Fig. 6e). mCherry-VHL deposition at INQ at 30 °C is explained by constitutive expression of GFP-Btn2, whereas endogenous Btn2 only accumulates upon heat shock (e.g. to 37 °C). In NLS-GFP expressing control cells, mCherry-VHL was diffusely distributed at 30 °C and proteotoxic stress triggered its nuclear accumulation in a diffused state, indicating preferential nuclear import under stress conditions consistent with former observations<sup>13,62,63</sup>. While GFP- $\alpha$ CLD and GFP-CTD did not allow for INQ formation of mCherry-VHL at 30 °C, some degree of nuclear mCherry-VHL foci formation became apparent after stress application (Fig. 5d). The partial stress-dependent mCherry-VHL sequestration mediated by GFP- $\alpha$ CLD or GFP-CTD can be likely explained by nuclear enrichment of mCherry-VHL upon heat shock. This will increase the local concentration of mCherry-VHL and thereby facilitate sequestration. The sequestrase activity of the GFP fusions to isolated  $\alpha$ CLD and CTD, however, was minor as compared to full-length Btn2, as judged by the fact that diffuse nuclear staining of mCherry-VHL was still present, in agreement with the phenotypes of respective deletion constructs.

The pattern of stress-induced mCherry-VHL foci formed in the presence of GFP- $\alpha$ CLD and GFP-CTD differed. GFP-CTD expression caused formation of multiple mCherry-VHL foci at the nuclear periphery, which, however, did not co-localize with GFP-CTD. While this finding points to a role of Btn2-CTD in INQ formation, in agreement with INQ deficiency of Btn2- $\Delta$ CTD-expressing cells, it does not allow to define a precise role. GFP- $\alpha$ CLD expression led to the formation of a single nuclear mCherry-VHL focus, which always co-localized with GFP- $\alpha$ CLD, suggesting sequestration of the reporter through direct GFP- $\alpha$ CLD interaction. We probed for mCherry-VHL interaction by isolating GFP-Btn2 fusion constructs after stress using GFP binder and testing for co-purified mCherry-VHL (Fig. 5e). mCherry-VHL was co-isolated with GFP-Btn2 and GFP- $\alpha$ CLD, but not GFP-CTD or the NLS-GFP control, demonstrating binding of  $\alpha$ CLD to the misfolded substrate.

We finally tested the ability of the Btn2 deletion constructs to restore growth of  $\Delta\Delta$  *btn2 $\Delta$*  cells at elevated temperatures (Fig. 5f). Btn2- $\Delta$  $\alpha$ CLD and Btn2- $\Delta$ CTD did not rescue the growth deficiency of  $\Delta\Delta$  *btn2 $\Delta$*  cells, mirroring their defects in INQ formation. Surprisingly, Btn2- $\Delta$ NTD-NLS did not only complement the growth defects of  $\Delta\Delta$  *btn2 $\Delta$*  cells, but even allowed for partial growth at 37 °C, which was not observed for  $\Delta\Delta$  reference cells expressing Btn2-wt (Fig. 5d). Btn2- $\Delta$ NTD-NLS therefore exhibits a gain-of-activity phenotype and is superior to





Btn2-wt if expressed in  $\Delta\Delta$  cells with low Hsp70 capacity. We assume that the underlying molecular basis is independent of sequestrase activities as (i) Btn2-wt and Btn2- $\Delta$ NTD-NLS do not differ in INQ formation (Fig. 5c) and (ii) both were expressed at comparable levels (Supplementary Fig. 6f). We instead speculate that differences in the susceptibility of INQ towards protein

disaggregases might explain the noticed differences between Btn2-wt and Btn2- $\Delta$ NTD-NLS in complementation behaviour.

**Btn2-NTD recruits disaggregases for INQ solubilization.** The above results prompted us to investigate whether Btn2-mediated

**Fig. 5** Characterization of Btn2 domains. **a** Btn2 consists of an N-terminal domain (NTD) harbouring a nuclear localization sequence (NLS), a  $\alpha$ -crystallin-like domain ( $\alpha$ CLD) and a disordered C-terminal domain (CTD). Protein disorder was predicted by IUPred and the relative abundance of hydrophobic and charged amino acids within each Btn2 domain was determined (right panel). The average abundance of respective amino acids in the yeast proteome is included as reference. **b** Partial proteolysis of Btn2 by subtilisin was analysed by SDS-PAGE. Btn2 degradation products were identified by mass spectrometry. **c** *Saccharomyces cerevisiae hsp42 $\Delta$  btn2 $\Delta$*  expressing the indicated Btn2 variants and mCherry-VHL as aggregation reporter were grown at 30 °C and heat shocked to 37 °C in the presence of MG132 for 90 min. Cellular localizations of mCherry-VHL were determined ( $n = 100$ , 2 replicates). DNA was stained by DAPI. **d** *Saccharomyces cerevisiae hsp42 $\Delta$  btn2 $\Delta$*  cells expressing mCherry-VHL and NLS-GFP or indicated NLS-GFP-Btn2 fusion constructs were grown at 30 °C and proteotoxic stress (37 °C + MG132) was applied for 90 min. Cellular localizations were determined and quantified ( $n = 100$  cells, 2 replicates). INQ: single GFP and mCherry-VHL foci; puncta: multiple mCherry-VHL foci that do not co-localize with GFP. **e** *Saccharomyces cerevisiae hsp42 $\Delta$  btn2 $\Delta$*  cells expressing mCherry-VHL and NLS-GFP or indicated NLS-GFP-Btn2 fusion constructs were exposed to proteotoxic stress (37 °C + MG132). GFP constructs were isolated using GFP-binder beads. The amount of precipitated GFP constructs and co-isolated mCherry-VHL was determined by western blot analysis. **f** Serial dilutions of indicated *S. cerevisiae* wild-type (wt) and chaperone mutant cells ( $\Delta\Delta$  *hsp104 $\Delta$  fes1 $\Delta$   $\Delta\Delta$  hsp104 $\Delta$  fes1 $\Delta$  btn2 $\Delta$* ) expressing the indicated Btn2 deletion variants were spotted on YPD plates and incubated at indicated temperatures for 2 days

sequestrations are reversed during recovery from stress, and if so, what the contribution of the Btn2 domains, especially of the NTD, to this process might be. We expressed Luciferase-DM-GFP-NLS as aggregation reporter in Btn2-wt- and Btn2- $\Delta$ NTD-NLS-expressing cells and subjected them to proteotoxic stress (37 °C + MG132) for 30 min. This caused strong reduction of Luciferase activity and sequestration into INQ, to similar extents for Btn2-wt- and Btn2- $\Delta$ NTD-NLS-expressing cells (Fig. 6a–c). To monitor the recovery of sequestered, pre-existing Luciferase-DM-GFP-NLS, we added cycloheximide at the end of the stress treatment to block de novo synthesis. The stress-inactivated Luciferase-DM-GFP-NLS regained 60% of its activity in Btn2-wt cells during a 60 min recovery period at 30 °C; this recovery was two-fold reduced for cells expressing Btn2- $\Delta$ NTD-NLS (Fig. 6a). To determine the contributions of the misfolded soluble and sequestered populations to Luciferase refolding, we repeated the recovery experiments in presence of low guanidinium hydrochloride (GdnHCl) concentrations (3 mM), which specifically inhibits the Hsp104 disaggregase<sup>64</sup>. The presence of GdnHCl reduced Luciferase refolding only in Btn2-wt-expressing cells but not in Btn2- $\Delta$ NTD-NLS-expressing cells, resulting in similar refolding yields for Btn2-wt- and Btn2- $\Delta$ NTD-NLS-expressing cells (Fig. 6a). This indicates that the increased Luciferase refolding yield in Btn2-wt cells stems from Hsp104-dependent INQ disaggregation. The partial regain of reporter activity in Btn2- $\Delta$ NTD-NLS-expressing cells instead stems from misfolded, yet soluble Luciferase-DM-GFP-NLS, which does not require Hsp104 activity for refolding.

This conclusion was confirmed when monitoring the fate of INQ-deposited Luciferase-DM-GFP-NLS in Btn2-wt- and Btn2- $\Delta$ NTD-NLS-expressing cells during the recovery phase (Fig. 6b, c). Nuclear Luciferase-DM-GFP-NLS sequestrations were efficiently removed at 30 °C within 60 min in Btn2-wt cells in an Hsp104-dependent manner, whereas they remained stable in Btn2- $\Delta$ NTD-NLS cells (Fig. 6b, c). This finding demonstrates that solubilization of Btn2-induced INQ requires the NTD of Btn2. Notably, nuclear aggregates of Luciferase-DM-GFP-NLS that formed infrequently in *btn2 $\Delta$*  cells were removed in an Hsp104-dependent manner, indicating that the disaggregation machinery does not require Btn2 per se (Supplementary Fig. 7a, b). Together, these findings indicate that the active sequestration of Luciferase-DM-GFP-NLS by Btn2 induces a strong dependence of the disaggregases on the Btn2-NTD.

To substantiate these findings, we used mCherry-VHL as alternative sequestration reporter (Supplementary Fig. 7c). We expressed mCherry-VHL in *hsp42 $\Delta$*  cells expressing Btn2-wt or Btn2- $\Delta$ NTD-NLS and induced INQ formation by proteotoxic stress (37 °C + MG132) for 90 min. Btn2-wt- and Btn2- $\Delta$ NTD-NLS-induced deposition of mCherry-VHL at INQ with similar efficiencies and both co-localized with the sequestered reporter (Supplementary Fig. 7c, d). During recovery (30 °C and MG132

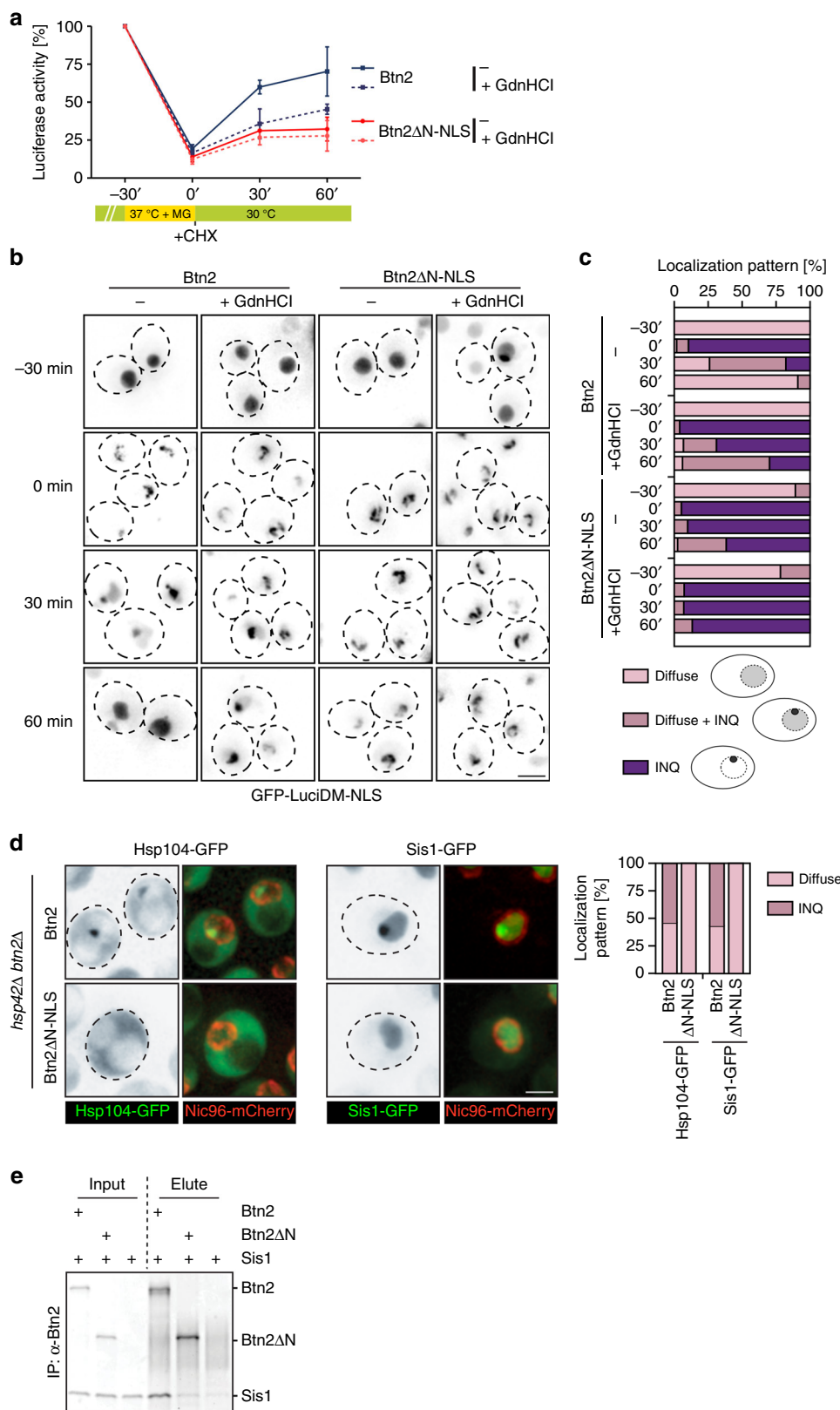
washout), mCherry-VHL foci were efficiently removed within 120 min in cells expressing Btn2-wt (Supplementary Fig. 7c), whereas they persisted in cells expressing Btn2- $\Delta$ NTD-NLS, confirming that the Btn2-NTD plays a crucial role in INQ disaggregation.

Btn2 accumulates only during the immediate phase of heat stress application, but is rapidly degraded afterwards<sup>12,13</sup>. We hypothesized that the Btn2- $\Delta$ NTD-NLS fragment is stabilized and consequently causes INQ persistence. We therefore compared the levels of Btn2 and Btn2- $\Delta$ NTD-NLS after heat shock and during the recovery period (Supplementary Fig. 7e). Btn2-wt and Btn2- $\Delta$ NTD-NLS accumulated to comparable levels upon heat shock and Btn2-wt rapidly vanished afterwards. The vast majority (71%) of Btn2- $\Delta$ NTD-NLS was also degraded upon stress relief (60 min at 30 °C), excluding the possibility that stabilization of Btn2- $\Delta$ NTD-NLS prevents INQ solubilization. However, a minor fraction (29%) of Btn2- $\Delta$ NTD-NLS remained stable throughout the recovery period (Supplementary Fig. 6E). We speculate that this fraction is protected from degradation because it is an integral part of the stabilized INQ. Accordingly, partial Btn2- $\Delta$ NTD-NLS stabilization is a consequence but not a cause of INQ persistence.

To address why the Btn2-NTD is crucial for INQ disaggregation, we tested whether it promotes direct interaction with components of the Hsp70-Hsp100 bi-chaperone disaggregase. We first monitored the localization of Hsp104-GFP in stressed *hsp42 $\Delta$*  cells expressing either Btn2-wt or Btn2- $\Delta$ NTD-NLS (Fig. 6d). Hsp104-GFP formed stress-induced nuclear INQ foci in the presence of Btn2-wt but not Btn2- $\Delta$ NTD-NLS, indicating that Hsp104 targeting to INQ is abolished (Fig. 6d, Supplementary Fig. 7f). Btn2- $\Delta$ NTD-NLS efficiently induced INQ formation under identical stress conditions (Fig. 5c, d), excluding differences in INQ formation as reason for the absence of Hsp104-GFP foci.

Hsp104 is recruited to protein aggregates by cooperation with Ssa1, which in turn requires Hsp40 co-chaperones for aggregate targeting<sup>65,66</sup>. Sis1 is a major Hsp40 in the nucleus of yeast<sup>62</sup> and cooperates with Ssa1 and Hsp104 in aggregate solubilization (Fig. 4d). We therefore tested for Sis1-GFP binding to INQ induced by either Btn2-wt or Btn2- $\Delta$ NTD-NLS (Fig. 6d, Supplementary Fig. 7f). Sis1 associated with INQ in the presence of Btn2-wt as revealed by formation of nuclear Sis1-GFP foci, but stayed diffuse in the nucleus in the presence of Btn2- $\Delta$ NTD-NLS. We infer that the yeast disaggregase (Hsp104/Ssa1/Sis1) does not bind INQ formed in the presence of Btn2- $\Delta$ NTD-NLS, explaining INQ persistence.

The determined binding deficiency of Sis1 suggests a physical interaction between Sis1 and the Btn2-NTD. Indeed, Sis1 physically interacted with Btn2-wt but not Btn2- $\Delta$ NTD *in vitro*, demonstrating that NTD mediated interaction of both proteins (Fig. 6e). Ydj1, the major yeast Hsp40 co-chaperone, did not



interact with Btn2 (Supplementary Fig. 7g), excluding that Sis1 recognizes Btn2 as misfolded protein. The specific Btn2-Sis1 interaction is in agreement with former findings<sup>12</sup>. Yet, we place the interaction of both chaperones in a distinct cellular context by showing that it is required for recruitment of the yeast Hsp70-Hsp100 disaggregase to ensure rapid INQ solubilization during

recovery phases. The Btn2-NTD-mediated recruitment of Sis1 and consequently Ssa1 can explain the superior growth complementation of  $\Delta\Delta$  cells by Btn2- $\Delta$ NTD-NLS (Fig. 5f): the Btn2 mutant does not recruit Hsp70 to INQ, thereby further increasing Hsp70 capacity and improving growth at increased temperatures in cells with low Hsp70 capacity.

**Fig. 6** The Btn2-NTD recruits disaggregases for INQ solubilization. **a–c** *Saccharomyces cerevisiae hsp42Δ* cells expressing GFP-LuciDM-NLS and Btn2 or Btn2ΔN-NLS were grown at 30 °C and exposed to proteotoxic stress for 30 min (37 °C + MG132). Cycloheximide (CHX) was added upon shifting cells back to 30 °C. Luciferase activities and cellular localizations were determined and quantified ( $n = 100$ ) at indicated time points. Luciferase activities prior to stress application were set to 100% and standard deviations were calculated based on three replicates. The Hsp104 disaggregase was inhibited by growing cells in presence of 3 mM guanidinium hydrochloride (GdnHCl). GFP-LuciDM-NLS localizations were determined at the indicated time points (**b**) and quantified (**c**) for  $n = 100$  cells and 2 replicates. **d** *Saccharomyces cerevisiae hsp42Δ* cells expressing Btn2 or Btn2ΔN-NLS and either Hsp104-GFP or Sis1-GFP were grown at 30 °C and exposed to proteotoxic stress (37 °C + MG132). Cellular localizations of Hsp104-GFP and Sis1-GFP were determined ( $n = 100$ , 2 replicates). The nuclear envelope was labelled by coexpression of fluorescent Nic96-mCherry nucleoporin. **e** Sis1 was incubated with Btn2 or Btn2ΔN and Btn2 was isolated by the addition of Btn2-binder beads. Input and bound fractions were analysed by SDS-PAGE followed by SYPRO-Ruby staining

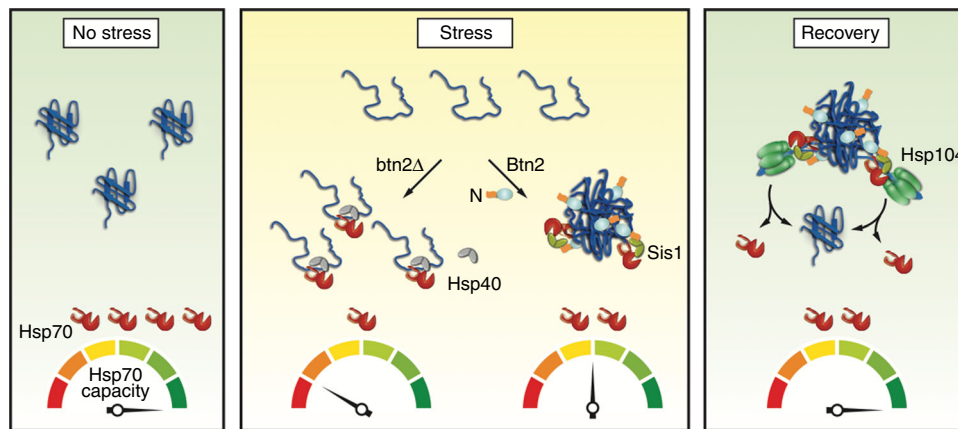


**Fig. 7** Btn2 sequestrase prevents Hsp70 overload during stress. Non-stressed cells have a high Hsp70 capacity, which is strongly reduced upon stress application by accumulating soluble misfolded proteins. Btn2 sequesters misfolded proteins into large assemblies and attenuates drop of Hsp70 capacity. The Btn2 N-terminal domain (N) recruits the cellular disaggregation machinery (Hsp70/Hsp104) by interacting with the Hsp70 co-chaperone Sis1. This ensures rapid reflux of sequestered proteins into the proteostasis network during recovery periods

## Discussion

The organized sequestration of misfolded proteins by specialized chaperones termed sequestrases is only recently realized as third pillar of protein quality control, next to refolding and degrading pathways. Here, we position this activity within the proteostasis network of yeast cells, demonstrate its crucial cytoprotective function and the direct, functional, and physical linkage of sequestrases to the Hsp70 system.

We show that the sequestrases Btn2 and Hsp42 become essential for yeast growth upon genetically limiting the capacity of Hsp70. Sequestration most likely shields sticky surfaces of misfolded proteins, thereby decreasing the number of available binding sites for Hsp70. This seems to be a critical function during stress exposure of cells since it counteracts an overboarding titration of Hsp70 away from its cellular housekeeping functions such as de novo protein folding<sup>67</sup>. In consequence, sequestrase activity effectively prevents proteostasis collapse and ensures cell viability under stress (Fig. 7). Protein aggregation has been frequently observed in Hsp70 mutant cells<sup>68–71</sup>, but was viewed as disastrous consequence of proteostasis breakdown. We suggest that this event rather reflects an activated cellular emergency programme executed by the Hsp42 and Btn2 sequestrases. Btn2 and Hsp42 are strongly upregulated upon both heat shock and limitations of Hsp70 capacity (Fig. 1c)<sup>72–74</sup>. This further supports that sequestration is an immediate response to acute proteotoxic stress, counteracting Hsp70 depletion.

We observed a dominant role of Btn2 and nuclear sequestration in stress survival of *fes1Δ hsp104Δ* cells. Most likely, nuclear Hsp70 capacity is particularly limited in these cells as they lack the nuclear Hsp70 NEF, Fes1. Hsp70 limitations may directly impact nuclear functions such as cell cycle control and gene regulation<sup>75</sup>. Notably, in *sse1Δ hsp104Δ* cells, which lack the

cytosolic Hsp70 NEF, Sse1, cytosolic Hsp42 becomes the most important sequestrase (Supplementary Fig. 1b). The particular roles of Btn2 and Hsp42 thus match compartment-specific limitations of the Hsp70 system.

How does Btn2 execute sequestrase activity? We present a comprehensive structure–function analysis of Btn2. We show Btn2 has chaperone activity and shares characteristics with sHsps. It exerts a stand-alone sequestrase activity necessary and sufficient to organize protein sequestration without additional factors. Our analysis defines three Btn2 domains (NTD, αCLD, CTD) with distinct functions in INQ formation and solubilization. Attempts to purify Btn2-ΔαCLD and Btn2-ΔCTD remained unsuccessful and characterizing the functions of αCLD and CTD domains therefore relied on the in vivo analysis of respective deletion constructs. The αCLD and CTD are essential for INQ formation with the αCLD involved in substrate interaction. We note that Cur1, the yeast paralog of Btn2, is largely missing the CTD and, accordingly, is not required for INQ formation<sup>12</sup>. The CTD is largely disordered but its precise role in sequestration remains unknown. Frequently proteins with large disordered segments are involved in organized phase separation and sequestration processes<sup>18,76,77</sup> by undergoing multivalent interactions with themselves and other components. The CTD of Btn2 contains multiple small clusters of negatively and positively charged residues, which we speculate promote Btn2 self-interaction but also contacts with sequestered substrates.

The Btn2-NTD is not essential for INQ formation but required for INQ solubilization. The NTD specifically recruits the Hsp70 co-chaperone Sis1, thereby initializing a hierarchical binding cascade of Hsp70 and Hsp104, which together form the yeast disaggregase. Btn2 was previously shown to bind to the C-terminal dimerization motif of Sis1 that is non-essential for its co-

chaperone function<sup>12,78</sup>. Btn2-Sis1 interaction therefore employs domains that are not crucial for basic sequestrase (Btn2) or disaggregase (Sis1) activities.

The function of Btn2-NTD as binding partner for Sis1 demands for its exposure at the INQ surface. Btn2 seems to shield the INQ surface, as Sis1 cannot bind to INQ induced by Btn2- $\Delta$ NTD-NLS, although it can directly bind to protein aggregates *in vitro*<sup>45,79</sup>. Sis1 dependence on Btn2-NTD for INQ binding therefore indicates that sequestered substrates are not sufficiently accessible to allow for direct Sis1 binding. This INQ architecture provides specificity for Sis1 and Hsp70-Hsp104 disaggregases. This may impact fate decisions of INQ-sequestered substrates, which get a chance to refold upon disaggregation as shown here for Luciferase-DM-GFP-NLS. Accordingly, yeast endogenous proteins that become sequestered upon heat shock in the cytosol and the nucleus are disaggregated and refolded without degradation occurring during the recovery period<sup>5</sup>. The ability of Btn2 to provide Hsp70 selectivity, involving physical contacts with the Hsp40 co-chaperone, Sis1, is a rather unique feature since the cooperation between Hsp40/Hsp70 and classical sHsps does not require direct interactions<sup>55</sup>.

In summary, we show that the sequestrase Btn2 controls key aspects of nuclear protein sequestration. By sequestering misfolded proteins during acute stress periods, Btn2 prevents Hsp70 overload (Fig. 7). At the same time, it prepares the sequestered proteins for fast and efficient Hsp70-dependent recovery upon stress relief.

## Methods

**Yeast strains, plasmids and growth conditions.** All *S. cerevisiae* strains used in this study are derived from BY4741. Strains and used plasmids are listed in the Supplementary Table 1, and used primers are listed in Supplementary Table 2. Yeast gene deletions were performed using a PCR-based protocol<sup>80</sup>. Deletion cassettes harbouring different selection markers were constructed by PCR using specific primers containing homologous flanks (30–50 nucleotides) for the gene of interest. PCR products were transformed into yeast cells, which were subsequently plated on appropriate plates containing the antibiotics or lacking the corresponding amino acid for selection. Gene deletions were confirmed by PCR and western blot analysis.

Antibiotics were used at the following final concentrations: 300  $\mu$ g/ml (geneticin), 100  $\mu$ g/ml (nourseothricin) and 300  $\mu$ g/ml (hygromycin). Doxycycline was added in a final concentration of 10  $\mu$ g/ml. Yeast cultures were cultivated in liquid YPD media or SC media supplemented with 2% glucose or 2% galactose/raffinose. The corresponding solid media contained 2% (w/v) agar. Yeast cultures were grown at 25 °C or at otherwise indicated growth conditions.

**Growth assays.** For spot test yeast cells were grown in SC or YPD medium to log phase (optical density at wavelength 600 nm ( $OD_{600}$ ) = 0.6–0.8) and then diluted to  $OD_{600}$  = 0.2. Cells were 5-fold serially diluted and spotted on YPD or SC agar plates. Plates were incubated at diverse temperatures for 2 days before documentation.

For recording growth curves yeast cells were grown in SC or YPD medium to log phase. Cells were diluted to  $OD_{600}$  = 0.2 and aliquoted into a 24-well plate. Yeast growth curves were measured in a temperature-controlled microplate reader (SPECTROstar Nano, BMG Labtech).

**Biochemical assays.** Hsp104, Ssa1, Sis1, Ydj1, Fes1 and Luciferase were purified from *E. coli* BL21 (NEB) or XL1 blue (lab stock) cells<sup>45,81</sup>. Hsp42 was purified from *E. coli* ArcticExpress cells (Agilent). All proteins were produced in cells grown at 30 °C, except for Luciferase and Hsp42, which were produced at 16 or 13 °C, respectively. Ssa1 and Fes1 were produced as His<sub>6</sub>-SUMO fusion constructs, and Hsp42 was produced as MBP (maltose-binding protein) fusion construct. Hsp104 and Luciferase-harboured C-terminal His<sub>6</sub> tags and were purified by Protino Ni-IDA resin in LEW buffer (50 mM NaH<sub>2</sub>PO<sub>4</sub> pH 8.0, 300 mM NaCl, 5 mM  $\beta$ -mercaptoethanol) and Superdex S200 size-exclusion chromatography in buffer A (50 mM HEPES, pH 7.6, 150 mM KCl, 20 mM MgCl<sub>2</sub>, 2 mM dithiothreitol (DTT)) supplemented with 5% (v/v) glycerol. His<sub>6</sub>-tagged Ydj1 and Sis1 were purified by Protino Ni-IDA resin in LEW buffer. His<sub>6</sub>-SUMO-Ssa1 and His<sub>6</sub>-SUMO-Fes1 were purified by Protino Ni-IDA resin in LWB150 buffer (40 mM HEPES, pH 7.4, 150 mM KCl, 5 mM MgCl<sub>2</sub>, 10 mM  $\beta$ -mercaptoethanol, 5% (v/v) glycerol). Eluted proteins were dialysed against LWB150 in the presence of His<sub>6</sub>-Ulp1 at 4 °C overnight to cleave off His<sub>6</sub>-SUMO. His<sub>6</sub>-SUMO and His<sub>6</sub>-Ulp1 were renived by incubation with Protino Ni-IDA resin. MBP-Hsp42 was purified by amylose resin

(NEB) in Hsp42 buffer (50 mM Tris, pH 7.5, 200 mM NaCl, 2 mM DTT, 10% (v/v) glycerol). Eluted proteins were dialysed overnight in the presence of PreScission protease (Sigma) to cleave of MBP. Hsp42 was finally purified by Sephacryl S-300 size-exclusion chromatography in Hsp42 buffer. Malate dehydrogenase was purchased from Roche, and pyruvate kinase was purchased from Sigma-Aldrich. Btn2 and Btn2 $\Delta$ N were produced as His<sub>6</sub>-SUMO fusion proteins in *E. coli* BL21DE3 (NEB) harbouring pCool6-Btn2 or pCool6-Btn2 $\Delta$ N. Cells were lysed in LEW buffer (50 mM NaH<sub>2</sub>PO<sub>4</sub> pH 8.0, 300 mM NaCl, 1 mM DTT) and incubated with Protino Ni-IDA resin. Btn2 and Btn2 $\Delta$ N were eluted from the resin by His<sub>6</sub>-Ulp1 cleavage in LEW buffer containing 50 mM NaCl. Btn2 and Btn2 $\Delta$ N were further purified by anion exchange column (Resource Q, Amersham) using a linear NaCl gradient (50–550 mM NaCl in LEW buffer) and size-exclusion chromatography (Superdex 200, Amersham) in LEW buffer.

For determining the impact of Btn2 on protein aggregation, 0.1  $\mu$ M Luciferase or 0.5  $\mu$ M MDH were incubated alone or in the presence of Btn2 at 43 and 41 °C, respectively, in buffer B (50 mM HEPES, pH 7.6, 50 mM KCl, 5 mM MgCl<sub>2</sub>, 2 mM DTT). Protein aggregation was monitored by determining sample turbidity at 600 nm using a Perkin-Elmer luminescence spectrometer LS50B.

Protein aggregates or complexes with Btn2 were analysed by glycerol gradient centrifugation. Luciferase (0.1  $\mu$ M) or MDH (0.5  $\mu$ M) were incubated at 43 or 41 °C for 15 and 60 min, respectively, in the absence or presence of Btn2. Protein samples (100  $\mu$ l) were overlaid on top of a 10–50% glycerol gradient in buffer A containing 1  $\mu$ M bovine serum albumin (BSA). Samples were centrifuged at 215,000  $\times$  g for 1 h at 4 °C (SW60 rotor). Fractions (500  $\mu$ l) were collected and analysed by sodium dodecyl sulfate-polyacrylamide gel electrophoresis (SDS-PAGE) followed by western blot analysis.

The impact of Btn2 and Hsp42 on substrate recovery was determined in disaggregation assays. Luciferase (0.1  $\mu$ M) was incubated at 43 °C for 15 min in buffer A in the absence and presence of 0.5  $\mu$ M Hsp42 or 2  $\mu$ M Btn2. Samples were shifted to 30 °C and mixed with disaggregating chaperones (2  $\mu$ M Ssa1, 1  $\mu$ M Sis1, 1  $\mu$ M Fes1, 1  $\mu$ M Hsp104, 50 nM final concentration of Luciferase) together with an ATP regenerating system (2 mM ATP, 3 mM phosphoenolpyruvate, 20 ng/ml pyruvate kinase). Luciferase activities were determined using the Lumat LB 9507.

In limited proteolysis experiments, 8  $\mu$ g Btn2 and 5 ng subtilisin (Boehringer) in 20  $\mu$ l reaction in buffer B (50 mM Tris, pH 7.5, 150 mM NaCl, 5 mM MgCl<sub>2</sub>, 1 mM DTT) were incubated at 25 °C for 2 h. Protease-resistant fragments were analysed by SDS-PAGE followed by Coomassie staining. Fragment identities were determined by mass spectrometry after tryptic digest.

Interaction of Btn2 and Sis1 was monitored in pull-down assays. One micromolar Btn2, Btn2 $\Delta$ N, Sis1 or Ydj1 were incubated in buffer A containing cComplete Protease Inhibitor (Sigma-Aldrich) at 25 °C for 15 min before mixing with 10  $\mu$ l Btn2-binder beads (Btn2 antibodies conjugated to NHS-activated sepharose beads (GE Healthcare)) for 15 min. The Btn2-binder beads were washed seven times with buffer A. Bound proteins were eluted by boiling in SDS sample buffer and analysed by SDS-PAGE stained by SYPRO-Ruby (Thermo Fisher Scientific).

Western blot analysis was performed as follows: SDS-PAGEs were transferred to PVDF membranes by semi-dry blotting. Membranes were subsequently blocked with 3% BSA (w/v) in TBS-T (Tris-buffered saline with Tween-20). Antibodies and used dilutions are listed in Supplementary Table 3 Anti-rabbit alkaline phosphatase conjugate (Vector Laboratories) was used as secondary antibody (1:20,000). Blots were developed using ECF™ Substrate (GE Healthcare) as reagent and imaged via Image-Reader LAS-4000 (Fujifilm). Western blotting was performed in two or more independent experiments each and representative results are provided.

**FACS analysis.** To monitor Hsf1-dependent gene expression, GFP was placed under the control of the *btn2* promoter. To increase reporter sensitivity, the unstable N-terminal domain of Btn2 was fused C-terminally to GFP. GFP fluorescence (excitation: 488 nm; emission: 530 nm) was determined by FACS (fluorescence-activated cell sorting) using the BD FACS Canto machine. Cultures of yeast strains were grown at 25 or 30 °C until log phase (0.6–0.8 OD). Two hundred microliters of cell culture was added to a flat-bottom 96-well plate with eight technical replicates per strain. FACS measured GFP fluorescence of 10,000 cells per strain. The GFP values were normalized by subtracting the values of a negative control.

**Negative staining and electron microscopy.** Protein samples were adsorbed to glow-discharged carbon-coated EM grids for 1 min. Grids were washed with distilled water and then stained with freshly prepared 2% uranyl-formiate (two passages). Micrographs were taken at pixel sizes of 0.36 nm using a Zeiss EM912 electron microscope (Carl Zeiss, Oberkochen, Germany) equipped with a cooled CCD camera (Proscan, München, Germany).

**Immunoprecipitation.** Fifty milliliters of yeast culture was grown at 30 °C to mid-log-phase and cells were harvested. Cell pellets were resuspended in 500  $\mu$ l IP buffer (50 mM Tris, pH 7.5, 150 mM NaCl, 5 mM MgCl<sub>2</sub>, 0.1% (v/v) TX-100, 5% (v/v) glycerol, 1 mM DTT, 2 mM phenylmethanesulfonyl fluoride, cComplete Protease Inhibitor) and lysed by bead beater (FastPrep-24, speed 6.5, 30 s, 6 repeats). After

removing the cell debris, 2 mg of total protein was incubated with 50  $\mu$ l GFP-binder beads in 1 ml IP buffer at 4 °C for 1 h. The beads were washed 7 $\times$  with IP buffer and bound proteins were eluted by boiling in SDS sample buffer. The amount of precipitated GFP and co-precipitated mCherry-VHL were monitored by western blotting using specific antibodies.

**Microscopy and image processing.** For live cell imaging, yeast cells were harvested by centrifugation, resuspended in SC medium and directly applied onto microscope slides. For DAPI (4',6-diamidino-2-phenylindole) staining, cells were first fixed with cold 70% ethanol for 5 min, washed once with H<sub>2</sub>O, followed by incubation with 50 ng/ml DAPI in phosphate-buffered saline (PBS). To collect cell images, optical sections of 0.2  $\mu$ m were acquired to image the whole-cell volume using a widefield system (xCellence IX81, Olympus) equipped with a Plan-Apochromat  $\times$ 100/NA 1.45 oil immersion objective and an EMCCD camera (Hamamatsu). Acquired z-stacks were deconvolved with xCellence software (Olympus) using the Wiener filter. All further processing and analysis of digital images was performed with ImageJ (NIH).

**Immunofluorescence microscopy.** Immunostaining was performed as previously described<sup>13</sup>. In brief, yeast cells were fixed with 4% (v/v) *p*-formaldehyde/100 mM KPO<sub>4</sub> (Sigma-Aldrich) for 1 h followed by cell wall digestion by 500  $\mu$ g/ml Zymolase T-100 in wash buffer (1.2 M sorbitol/100 mM KPO<sub>4</sub>, pH 6.5) supplemented with 20 mM  $\beta$ -mercaptoethanol for 30 min at 30 °C. Spheroblasts were attached to poly-lysine-coated cover slides, permeabilized by washing three times with 1% (v/v) Triton X-100/100 mM KPO<sub>4</sub>, pH 6.5 and blocked for 1 h with 1% (w/v) BSA in 100 mM KPO<sub>4</sub>, pH 6.5. All antibodies were diluted in blocking buffer. Primary and secondary antibody incubations were carried out for 1 h at room temperature. Afterwards, spheroblasts were stained with 100 ng/ml DAPI in PBS and embedded in 50% glycerol. Antibodies and used dilutions are listed in Supplementary Table 2.

### Data availability

The source data underlying Figs. 1c, 2c, 4, 4b–f, 5e, 6a, e, Supplementary Figs. 1c, e, 2a–c, e, 3b, d, e, 4a, e, 5c, d, 6b, d, f, 7e, g are provided as a Source data file. Other data are available from the corresponding authors upon reasonable request.

Received: 20 December 2018; Accepted: 7 October 2019;

Published online: 24 October 2019

### References

- Walther, D. M. et al. Widespread proteome remodeling and aggregation in aging *C. elegans*. *Cell* **161**, 919–932 (2015).
- David, D. C. et al. Widespread protein aggregation as an inherent part of aging in *C. elegans*. *PLoS Biol.* **8**, e1000450 (2010).
- Gupta, R. et al. Firefly luciferase mutants as sensors of proteome stress. *Nat. Methods* **8**, 879–884 (2011).
- Ben-Zvi, A., Miller, E. A. & Morimoto, R. I. Collapse of proteostasis represents an early molecular event in *Caenorhabditis elegans* aging. *Proc. Natl Acad. Sci. USA* **106**, 14914–14919 (2009).
- Wallace, E. W. et al. Reversible, specific, active aggregates of endogenous proteins assemble upon heat stress. *Cell* **162**, 1286–1298 (2015).
- Cherkasov, V. et al. Systemic control of protein synthesis through sequestration of translation and ribosome biogenesis factors during severe heat stress. *FEBS Lett.* **589**, 3654–3664 (2015).
- Kaganovich, D., Kopito, R. & Frydman, J. Misfolded proteins partition between two distinct quality control compartments. *Nature* **454**, 1088–1095 (2008).
- Johnston, J. A., Ward, C. L. & Kopito, R. R. Aggresomes: a cellular response to misfolded proteins. *J. Cell Biol.* **143**, 1883–1898 (1998).
- Tyedmers, J., Mogk, A. & Bukau, B. Cellular strategies for controlling protein aggregation. *Nat. Rev. Mol. Cell Biol.* **11**, 777–788 (2010).
- Kawaguchi, Y. et al. The deacetylase HDAC6 regulates aggresome formation and cell viability in response to misfolded protein stress. *Cell* **115**, 727–738 (2003).
- Specht, S., Miller, S. B., Mogk, A. & Bukau, B. Hsp42 is required for sequestration of protein aggregates into deposition sites in *Saccharomyces cerevisiae*. *J. Cell Biol.* **195**, 617–629 (2011).
- Malinowska, L., Kroschwald, S., Munder, M. C., Richter, D. & Alberti, S. Molecular chaperones and stress-inducible protein-sorting factors coordinate the spatiotemporal distribution of protein aggregates. *Mol. Biol. Cell* **23**, 3041–3056 (2012).
- Miller, S. B. et al. Compartment-specific aggregates direct distinct nuclear and cytoplasmic aggregate deposition. *EMBO J.* **34**, 778–797 (2015).
- Saarikangas, J. & Barral, Y. Protein aggregates are associated with replicative aging without compromising protein quality control. *eLife* **4**, <https://doi.org/10.7554/eLife.06197> (2015).
- Song, J. et al. Essential genetic interactors of SIR2 required for spatial sequestration and asymmetrical inheritance of protein aggregates. *PLoS Genet.* **10**, e1004539 (2014).
- Escusa-Toret, S., Vonk, W. I. & Frydman, J. Spatial sequestration of misfolded proteins by a dynamic chaperone pathway enhances cellular fitness during stress. *Nat. Cell Biol.* **15**, 1231–1243 (2013).
- Gallina, I. et al. Cmr1/WDR76 defines a nuclear genotoxic stress body linking genome integrity and protein quality control. *Nat. Commun.* **6**, 6533 (2015).
- Grousl, T. et al. A prion-like domain in Hsp42 drives chaperone-facilitated aggregation of misfolded proteins. *J. Cell Biol.* **217**, 1269–1285 (2018).
- Chen, B., Retzlaff, M., Roos, T. & Frydman, J. Cellular strategies of protein quality control. *Cold Spring Harb. Perspect. Biol.* **3**, a004374 (2011).
- Hill, S. M., Hanzen, S. & Nystrom, T. Restricted access: spatial sequestration of damaged proteins during stress and aging. *EMBO Rep.* **18**, 377–391 (2017).
- Miller, S. B., Mogk, A. & Bukau, B. Spatially organized aggregation of misfolded proteins as cellular stress defense strategy. *J. Mol. Biol.* **427**, 1564–1574 (2015).
- Arrasate, M., Mitra, S., Schweitzer, E. S., Segal, M. R. & Finkbeiner, S. Inclusion body formation reduces levels of mutant huntingtin and the risk of neuronal death. *Nature* **431**, 805–810 (2004).
- Cheng, I. H. et al. Accelerating amyloid-beta fibrillization reduces oligomer levels and functional deficits in Alzheimer disease mouse models. *J. Biol. Chem.* **282**, 23818–23828 (2007).
- Cohen, E., Bieschke, J., Perciavalle, R. M., Kelly, J. W. & Dillin, A. Opposing activities protect against age-onset proteotoxicity. *Science* **313**, 1604–1610 (2006).
- Cohen, E. et al. Reduced IGF-1 signaling delays age-associated proteotoxicity in mice. *Cell* **139**, 1157–1169 (2009).
- Wolfe, K. J., Ren, H. Y., Trepte, P. & Cyr, D. M. The Hsp70/90 cochaperone, Sti1, suppresses proteotoxicity by regulating spatial quality control of amyloid-like proteins. *Mol. Biol. Cell* **24**, 3588–3602 (2013).
- Liu, B. et al. The polarisome is required for segregation and retrograde transport of protein aggregates. *Cell* **140**, 257–267 (2010).
- Zhou, C. et al. Organelle-based aggregation and retention of damaged proteins in asymmetrically dividing cells. *Cell* **159**, 530–542 (2014).
- Spokoini, R. et al. Confinement to organelle-associated inclusion structures mediates asymmetric inheritance of aggregated protein in budding yeast. *Cell Rep.* **2**, 738–747 (2012).
- Marshall, R. S., McLoughlin, F. & Vierstra, R. D. Autophagic Turnover of inactive 26S proteasomes in yeast is directed by the ubiquitin receptor Cue5 and the Hsp42 chaperone. *Cell Rep.* **16**, 1717–1732 (2016).
- Xie, Y. & Varshavsky, A. RPN4 is a ligand, substrate, and transcriptional regulator of the 26S proteasome: a negative feedback circuit. *Proc. Natl Acad. Sci. USA* **98**, 3056–3061 (2001).
- Kusmierczyk, A. R., Kunjappu, M. J., Funakoshi, M. & Hochstrasser, M. A multimeric assembly factor controls the formation of alternative 20S proteasomes. *Nat. Struct. Mol. Biol.* **15**, 237–244 (2008).
- Wang, X., Xu, H., Ju, D. & Xie, Y. Disruption of Rpn4-induced proteasome expression in *Saccharomyces cerevisiae* reduces cell viability under stressed conditions. *Genetics* **180**, 1945–1953 (2008).
- Eisele, F. & Wolf, D. H. Degradation of misfolded protein in the cytoplasm is mediated by the ubiquitin ligase Ubr1. *FEBS Lett.* **582**, 4143–4146 (2008).
- Heck, J. W., Cheung, S. K. & Hampton, R. Y. Cytoplasmic protein quality control degradation mediated by parallel actions of the E3 ubiquitin ligases Ubr1 and San1. *Proc. Natl Acad. Sci. USA* **107**, 1106–1111 (2010).
- Gardner, R. G., Nelson, Z. W. & Gottschling, D. E. Degradation-mediated protein quality control in the nucleus. *Cell* **120**, 803–815 (2005).
- Fang, N. N. et al. Rsp5/Nedd4 is the main ubiquitin ligase that targets cytosolic misfolded proteins following heat stress. *Nat. Cell Biol.* **16**, 1227–1237 (2014).
- Balchin, D., Hayer-Hartl, M. & Hartl, F. U. In vivo aspects of protein folding and quality control. *Science* **353**, aac4354 (2016).
- Nillegoda, N. B., Wentink, A. S. & Bukau, B. Protein disaggregation in multicellular organisms. *Trends Biochem. Sci.* **43**, 285–300 (2018).
- Kabani, M., Beckerich, J. M. & Brodsky, J. L. Nucleotide exchange factor for the yeast Hsp70 molecular chaperone Ssa1p. *Mol. Cell Biol.* **22**, 4677–4689 (2002).
- Glover, J. R. & Lindquist, S. Hsp104, Hsp70, and Hsp40: novel chaperone system that rescues previously aggregated proteins. *Cell* **94**, 73–82 (1998).
- Rosenzweig, R., Moradi, S., Zarrine-Afsar, A., Glover, J. R. & Kay, L. E. Unraveling the mechanism of protein disaggregation through a ClpB-DnaK interaction. *Science* **339**, 1080–1083 (2013).
- Zheng, X. et al. Dynamic control of Hsf1 during heat shock by a chaperone switch and phosphorylation. *eLife* **5**, <https://doi.org/10.7554/eLife.18638> (2016).
- Solis, E. J. et al. Defining the essential function of yeast hsf1 reveals a compact transcriptional program for maintaining eukaryotic proteostasis. *Mol. Cell* **63**, 60–71 (2016).

45. Ungelenk, S. et al. Small heat shock proteins sequester misfolding proteins in near-native conformation for cellular protection and efficient refolding. *Nat. Commun.* **7**, 13673 (2016).
46. Raviol, H., Sadlish, H., Rodriguez, F., Mayer, M. P. & Bukau, B. Chaperone network in the yeast cytosol: Hsp110 is revealed as an Hsp70 nucleotide exchange factor. *EMBO J.* **25**, 2510–2518 (2006).
47. Dragovic, Z., Broadley, S. A., Shomura, Y., Bracher, A. & Hartl, F. U. Molecular chaperones of the Hsp110 family act as nucleotide exchange factors of Hsp70s. *EMBO J.* **25**, 2519–2528 (2006).
48. Kaimal, J. M., Kandasamy, G., Gasser, F. & Andreasson, C. Coordinated Hsp110 and Hsp104 activities power protein disaggregation in *Saccharomyces cerevisiae*. *Mol. Cell. Biol.* <https://doi.org/10.1128/MCB.00027-17> (2017).
49. Gowda, N. K. et al. Cytosolic splice isoform of Hsp70 nucleotide exchange factor Fes1 is required for the degradation of misfolded proteins in yeast. *Mol. Biol. Cell* **27**, 1210–1219 (2016).
50. Garcia, V. M., Nillegoda, N. B., Bukau, B. & Morano, K. A. Substrate binding by the yeast Hsp110 nucleotide exchange factor and molecular chaperone Sse1 is not obligate for its biological activities. *Mol. Biol. Cell* **28**, 2066–2075 (2017).
51. McClellan, A. J., Scott, M. D. & Frydman, J. Folding and quality control of the VHL tumor suppressor proceed through distinct chaperone pathways. *Cell* **121**, 739–748 (2005).
52. Wickner, R. B., Bezsonov, E. & Bateman, D. A. Normal levels of the antiprion proteins Btn2 and Cur1 cure most newly formed [URE3] prion variants. *Proc. Natl Acad. Sci. USA* **111**, E2711–E2720 (2014).
53. Schröder, H., Langer, T., Hartl, F.-U. & Bukau, B. DnaK, DnaJ, GrpE form a cellular chaperone machinery capable of repairing heat-induced protein damage. *EMBO J.* **12**, 4137–4144 (1993).
54. Mogk, A. et al. Refolding of substrates bound to small Hsps relies on a disaggregation reaction mediated most efficiently by ClpB/DnaK. *J. Biol. Chem.* **278**, 31033–31042 (2003).
55. Zwirowski, S. et al. Hsp70 displaces small heat shock proteins from aggregates to initiate protein refolding. *EMBO J.* **36**, 783–796 (2017).
56. Haslbeck, M., Miess, A., Stromer, T., Walter, S. & Buchner, J. Disassembling protein aggregates in the yeast cytosol. The cooperation of Hsp26 with Ssa1 and Hsp104. *J. Biol. Chem.* **280**, 23861–23868 (2005).
57. Lee, U. et al. Genetic analysis reveals domain interactions of *Arabidopsis* Hsp100/ClpB and cooperation with the small heat shock protein chaperone system. *Plant Cell* **17**, 559–571 (2005).
58. Cashikar, A. G., Duennwald, M. & Lindquist, S. L. A chaperone pathway in protein disaggregation. Hsp26 alters the nature of protein aggregates to facilitate reactivation by Hsp104. *J. Biol. Chem.* **280**, 23869–23875 (2005).
59. Matuszewska, M., Kuczynska-Wisnik, D., Laskowska, E. & Liberek, K. The small heat shock protein IbpA of *Escherichia coli* cooperates with IbpB in stabilization of thermally aggregated proteins in a disaggregation competent state. *J. Biol. Chem.* **280**, 12292–12298 (2005).
60. Soding, J., Biegert, A. & Lupas, A. N. The HHpred interactive server for protein homology detection and structure prediction. *Nucleic Acids Res.* **33**, W244–W248 (2005).
61. Dosztanyi, Z., Csizmek, V., Tompa, P. & Simon, I. IUPred: web server for the prediction of intrinsically unstructured regions of proteins based on estimated energy content. *Bioinformatics* **21**, 3433–3434 (2005).
62. Park, S. H. et al. PolyQ proteins interfere with nuclear degradation of cytosolic proteins by sequestering the Sis1p chaperone. *Cell* **154**, 134–145 (2013).
63. Prasad, R., Kawaguchi, S. & Ng, D. T. A nucleus-based quality control mechanism for cytosolic proteins. *Mol. Biol. Cell* **21**, 2117–2127 (2010).
64. Jung, G., Jones, G. & Masison, D. C. Amino acid residue 184 of yeast Hsp104 chaperone is critical for prion-curing by guanidine, prion propagation, and thermotolerance. *Proc. Natl Acad. Sci. USA* **99**, 9936–9941 (2002).
65. Winkler, J., Tyedmers, J., Bukau, B. & Mogk, A. Hsp70 targets Hsp100 chaperones to substrates for protein disaggregation and prion fragmentation. *J. Cell Biol.* **198**, 387–404 (2012).
66. Acebron, S. P., Fernandez-Saiz, V., Taneva, S. G., Moro, F. & Muga, A. DnaJ recruits DnaK to protease aggregates. *J. Biol. Chem.* **283**, 1381–1390 (2008).
67. Rosenzweig, R., Nillegoda, N. B., Mayer, M. P. & Bukau, B. The Hsp70 chaperone network. *Nat. Rev. Mol. Cell. Biol.* <https://doi.org/10.1038/s41580-019-0133-3> (2019).
68. Gowda, N. K., Kandasamy, G., Froehlich, M. S., Dohmen, R. J. & Andreasson, C. Hsp70 nucleotide exchange factor Fes1 is essential for ubiquitin-dependent degradation of misfolded cytosolic proteins. *Proc. Natl Acad. Sci. USA* **110**, 5975–5980 (2013).
69. Abrams, J. L., Verghese, J., Gibney, P. A. & Morano, K. A. Hierarchical functional specificity of cytosolic heat shock protein 70 (Hsp70) nucleotide exchange factors in yeast. *J. Biol. Chem.* **289**, 13155–13167 (2014).
70. Shiber, A., Breuer, W., Brandeis, M. & Ravid, T. Ubiquitin conjugation triggers misfolded protein sequestration into quality-control foci when Hsp70 chaperone levels are limiting. *Mol. Biol. Cell* **24**, 2076–2087 (2013).
71. Park, S. H. et al. The cytoplasmic Hsp70 chaperone machinery subjects misfolded and endoplasmic reticulum import-incompetent proteins to degradation via the ubiquitin-proteasome system. *Mol. Biol. Cell* **18**, 153–165 (2007).
72. Gasch, A. P. et al. Genomic expression programs in the response of yeast cells to environmental changes. *Mol. Biol. Cell* **11**, 4241–4257 (2000).
73. Jarnuczak, A. F., Albornoz, M. G., Eyers, C. E., Grant, C. M. & Hubbard, S. J. A quantitative and temporal map of proteostasis during heat shock in *Saccharomyces cerevisiae*. *Mol. Omics* **14**, 37–52 (2018).
74. Nagaraj, N. et al. System-wide perturbation analysis with nearly complete coverage of the yeast proteome by single-shot ultra HPLC runs on a bench top Orbitrap. *Mol. Cell Proteom.* **11**, M11 013722 (2012).
75. Truman, A. W. et al. CDK-dependent Hsp70 phosphorylation controls G1 cyclin abundance and cell-cycle progression. *Cell* **151**, 1308–1318 (2012).
76. Malinowska, L., Kroschwald, S. & Alberti, S. Protein disorder, prion propensities, and self-organizing macromolecular collectives. *Biochim. Biophys. Acta* **1834**, 918–931 (2013).
77. Protter, D. S. & Parker, R. Principles and properties of stress granules. *Trends Cell Biol.* **26**, 668–679 (2016).
78. Reidy, M. et al. Hsp40s specify functions of hsp104 and hsp90 protein chaperone machines. *PLoS Genet.* **10**, e1004720 (2014).
79. Nillegoda, N. B. et al. Evolution of an intricate J-protein network driving protein disaggregation in eukaryotes. *eLife* **6**, <https://doi.org/10.7554/eLife.24560> (2017).
80. Janke, C. et al. A versatile toolbox for PCR-based tagging of yeast genes: new fluorescent proteins, more markers and promoter substitution cassettes. *Yeast* **21**, 947–962 (2004).
81. Rampelt, H. et al. Metazoan Hsp70 machines use Hsp110 to power protein disaggregation. *EMBO J.* **31**, 4221–4235 (2012).

## Acknowledgements

This work was supported by the Deutsche Forschungsgemeinschaft (SFB1036 project A8 to A.M. and B.B.). We acknowledge support of C.-t.H. by the Hartmut Hoffmann-Berling International Graduate School of Molecular and Cellular Biology (HBIGS) and A.J. by the Helmholtz International Graduate School for Cancer Research at the DKFZ. We thank Claes Andreasson for providing pSUMO-Fes1 and Kevin A. Morano for providing p413TEF-FLAG-Sse1sbd.

## Author contributions

Conceived and designed experiments: C.-t.H., T.G., O.S., A.J., C.R.-H., K.R., B.B., A.M. Performed experiments: C.-t.H., T.G., O.S., A.J., C.R.-H., M.S., R.Z., K.R. Analysed the data: C.-t.H., T.G., O.S., A.J., C.R.-H., M.S., K.R., B.B., A.M. Wrote the manuscript: B.B., A.M.

## Competing interests

The authors declare no competing interests.

## Additional information

**Supplementary information** is available for this paper at <https://doi.org/10.1038/s41467-019-12868-1>.

**Correspondence** and requests for materials should be addressed to B.B. or A.M.

**Peer review information** *Nature Communications* thanks the anonymous reviewer(s) for their contribution to the peer review of this work.

**Reprints and permission information** is available at <http://www.nature.com/reprints>

**Publisher's note** Springer Nature remains neutral with regard to jurisdictional claims in published maps and institutional affiliations.



**Open Access** This article is licensed under a Creative Commons Attribution 4.0 International License, which permits use, sharing, adaptation, distribution and reproduction in any medium or format, as long as you give appropriate credit to the original author(s) and the source, provide a link to the Creative Commons license, and indicate if changes were made. The images or other third party material in this article are included in the article's Creative Commons license, unless indicated otherwise in a credit line to the material. If material is not included in the article's Creative Commons license and your intended use is not permitted by statutory regulation or exceeds the permitted use, you will need to obtain permission directly from the copyright holder. To view a copy of this license, visit <http://creativecommons.org/licenses/by/4.0/>.

© The Author(s) 2019